

# Bayesian design optimization of fiber-based biomimetic soft actuators

Bartosz KaczmarSKI<sup>a</sup>, Derek E. Moulton<sup>b</sup>, Alain Goriely<sup>b</sup>, Ellen Kuhl<sup>a,\*</sup>

<sup>a</sup>*Living Matter Laboratory, Stanford University, Stanford, 94305, California, USA*

<sup>b</sup>*Mathematical Institute, University of Oxford, Oxford, OX2 6GG, United Kingdom*

---

## Abstract

Designing versatile soft actuators that achieve a satisfactory trade-off between robotic adaptability and structural complexity is an exceedingly difficult task. Most predominantly, researchers have used statistical and physics-based models to simulate the mechanical behavior of soft actuators. Such computational representations can be used to identify optimal actuator designs that fulfill user-specified robotic requirements. However, in trying to approach this actuator optimization problem, designers are often forced to either employ simplifying modeling assumptions that reduce predictive fidelity, or apply computationally expensive simulation frameworks that limit the extent of design space exploration. Here, we propose a generalized Bayesian optimization methodology for identifying designs of fiber-based biomimetic soft actuators that minimize the actuation energy under arbitrary robotic control requirements. Our approach is computationally inexpensive, as it quantifies the mechanics of the optimized fiber-based actuators by using the reduced-order active filament model. We evaluated our Bayesian optimization procedure for a simple control objective specification, in which the soft actuator's end effector is to reach a specified target position. We found that the proposed optimization methodology performs better than a random-search baseline, since it identifies more desirable actuator designs faster and more frequently. Even though the performance of our approach was evaluated for a single actuation paradigm and one set of design requirements, the methodology can be readily applied to the design optimization of fiber-based actuators under a large family of other robotic scenarios.

*Keywords:* Soft actuators, Automated design, Bayesian optimization, Continuum mechanics

---

## 1. Nomenclature

$A$	= Fourier amplitude quantity in the active filament formulae for $\hat{\mathbf{u}}$
$\mathbf{A}$	= elastic part in the multiplicative decomposition of $\mathbf{F}$
$\mathbb{A}$	= the general active filament model function taking $\Gamma$ and $\mathcal{P}$ as input, and outputting $\hat{\zeta}$ , $\hat{\mathbf{u}}$
$a_0, a_1, b_1$	= first three Fourier coefficients of $\gamma(\theta)$
$\mathcal{B}$	= domain $\mathcal{B} \subset \mathbb{R}^3$ of the undeformed configuration of the filament (before dimensional reduction)

---

\*Corresponding author

Email addresses: [bartoszk@stanford.edu](mailto:bartoszk@stanford.edu) (Bartosz KaczmarSKI), [moulton@maths.ox.ac.uk](mailto:moulton@maths.ox.ac.uk) (Derek E. Moulton), [alain.goriely@maths.ox.ac.uk](mailto:alain.goriely@maths.ox.ac.uk) (Alain Goriely), [ekuhl@stanford.edu](mailto:ekuhl@stanford.edu) (Ellen Kuhl)

$\mathcal{B}_{\mathbb{A}}$	= reduced deformed configuration $\{\mathbf{r}, \{\mathbf{d}_1, \mathbf{d}_3, \mathbf{d}_3\}\}$ of the filament upon fiber activation
$\mathcal{C}_{\bullet}$	= set of constraints imposed on object $\bullet$
$c_{\bullet}$	= an element of $\mathcal{C}_{\bullet}$
$\mathbf{D}$	= director basis map $\{\mathbf{d}_1, \mathbf{d}_3, \mathbf{d}_3\} : \mathbb{R} \rightarrow \{\mathbb{R}^3, \mathbb{R}^3, \mathbb{R}^3\}$ of the filament
$\mathcal{D}$	= set of parameters defining the filament geometry
$\mathbf{d}_i$	= $i$ -th vector in the director basis of the filament, $i \in \{1, 2, 3\}$ , $\mathbf{d}_i \in \mathbb{R}^3$
$E$	= Young's modulus of the filament
$\mathcal{E}^{\mathcal{G}}$	= energetic activation cost optimal under a control goal specification $\mathcal{G}$
$\mathbf{F}$	= deformation gradient tensor field
$\mathcal{F}$	= set of parameters defining the fiber architecture embedded in the filament
$f$	= objective function minimized via Bayesian optimization; an algorithmic augmentation of $\mathcal{E}^{\mathcal{G}}$
$f_{\text{best}}$	= function of $k$ returning the minimum value of $f$ found after $k$ iterations
$f_{\min}$	= minimum value of the objective function found so far in the Bayesian optimization process
$f_{\text{th}}$	= objective value threshold for the computation of the $\mathcal{K}_{\min}$ metric
$\mathbf{G}$	= 3-dimensional tensor field of rank 2 defining the fibrillar activation along $\mathbf{m}$ throughout $\mathcal{B}$
$\mathcal{G}$	= definition of the control goal
$\mathcal{G}$	= complete specification of the control objective, with all auxiliary objects
$\text{GC}$	= a boolean flag that is <code>true</code> whenever the actuator exhibits satisfactory control
$\text{GP}$	= a Gaussian Process object
$H$	= complete evaluation history of points $(\mathcal{P}, f)$ in the GP
$\text{Imp}$	= improvement function used in the maximization of the expectation $\mathbb{E}[\text{Imp}]$
$J^{\mathcal{G}}$	= cost function associated with control goal $\mathcal{G}$
$K$	= number of iterations in the Bayesian optimization algorithm
$K_d$	= number of iteration windows for which the distributions of function evaluations are computed
$\mathcal{K}_{\min}$	= minimum iteration index $k$ for which $f_{\text{best}}(k)$ is smaller than some threshold $f_{\text{th}}$
$k_{\text{GP}}$	= kernel function used in the GP
$L$	= length of the actuator; the same for all rings
$M$	= total number of rings in a multi-ring filament
$\mathcal{M}_{\mathbb{E}}$	= optimization scheme used for expected improvement maximization
$\mathcal{M}_{\Gamma}$	= optimization scheme in the algorithm for activation optimization; default is Nelder-Mead
$\mathbf{m}$	= 3-dimensional vector field defining the fiber directions throughout $\mathcal{B}$
$N$	= number of active angular sectors in the piecewise definition of $\gamma(\theta)$
$\mathcal{N}$	= normal distribution; $\mathcal{N}(x   \mu, \sigma^2)$ is a normal PDF with mean $\mu$ and standard deviation $\sigma$
$N_{\text{res}}$	= maximum number of restarts of $\mathcal{M}_{\mathbb{E}}$ permitted for identifying a satisfactory evaluation point
$n_{\text{core}}$	= number of CPU cores available
$n_{\mathbb{E}}$	= number of samples in the initial interior sampling plan used in the chosen scheme for $\mathcal{M}_{\mathbb{E}}$
$n_{\text{init}}$	= number of initial points (at each $f$ evaluation) provided for the activation optimization algorithm
$n_{\text{prior}}$	= number of prior data points after post-processing

$n_{\text{rand}}$	=	number of samples used for the random baseline in performance evaluation
$\tilde{n}_{\text{prior}}$	=	number of data points used to initialize the sampling plan for prior generation
$O$	=	set of auxiliary optimization hyperparameters
$\mathcal{P}$	=	set of all parameters defining the active filament
$\mathcal{P}_i^{\text{near}}$	=	$i$ -th closest point to some point $\mathcal{P}$ in $L_2$ -norm
$R_0$	=	outer radius of the entire filament
$R_1, R_2$	=	inner and outer radii of the cylindrical filamentary tube defining a given ring
$\mathcal{R}$	=	a tubular (ring) region in the simplified cylindrical geometry of the filament
$\mathbf{r}$	=	filament centerline map (an $\mathbb{R} \rightarrow \mathbb{R}^3$ space curve)
$S$	=	random seed used in the initialization of $\mathcal{M}_{\Gamma}$
$\mathcal{S}$	=	set of arc length values for a given target curve in $\mathcal{G}$ over which $J^{\mathcal{G}}$ is defined
$t$	=	thickness of the annular cross-section of the filamentary tube
$\mathcal{U}$	=	continuous uniform distribution; $\mathcal{U}(a, b)$ , $a, b \in \mathbb{R}^n$ , corresponds to $\prod_{i=1}^n \mathcal{U}(a_i, b_i)$
$\mathbf{u}$	=	vector $(u_1, u_2, u_3)$ , where $u_i$ is the curvature function of the filament around the axis defined by $\mathbf{d}_i$
$\hat{\mathbf{u}}$	=	intrinsic version of $\mathbf{u}$
$v_{ij}$	=	weight in $J^{\mathcal{G}}$ corresponding to $\mathbf{d}_j$ , and the $i$ -th element of $\mathcal{Z}$ and $\mathcal{S}$
$w_i$	=	weight in $J^{\mathcal{G}}$ corresponding to $\mathbf{r}$ , and the $i$ -th element of $\mathcal{Z}$ and $\mathcal{S}$
$\mathcal{X}_{\bullet}$	=	feasible set corresponding to the object $\bullet$
$Z$	=	material parameter and the argument of $\mathcal{B}_{\mathbb{A}}$
$\mathcal{X}_{\text{prior}}$	=	quasi-random sampling plan for prior generation
$\mathcal{X}_{\text{GP}}$	=	sampling plan for expected improvement maximization
$\mathbf{Z}_{\text{min/max}}$	=	set of all minimum/maximum perturbation vectors $\mathbf{z}_{\text{min/max}}^{(i)}$ , $i \in \{1, \dots, M\}$
$\mathcal{Z}$	=	set of material parameters $Z$ over which the cost function $J^{\mathcal{G}}$ is defined
$\mathbf{z}_{\text{min/max}}$	=	vector in $\mathbb{R}^N$ of minimum/maximum perturbations of $\gamma$ (for parallelized initializations)
$\alpha_2$	=	helical angle of the fiber field at $R = R_2$ (the outer surface of the filamentary tube)
$\Gamma$	=	vector of all $\gamma^{(i)}$ , $i \in \{1, \dots, M\}$
$\gamma$	=	piecewise function defining the cross-sectional activation distribution in a fiber field of a single ring
$\gamma_i$	=	fiber activation parameter corresponding to the $i$ -th annular sector in the piecewise definition of $\gamma(\theta)$
$\gamma_0$	=	scalar factor in $[0, 1]$ used in linear interpolation of the control path in the $\gamma$ -space
$\boldsymbol{\Gamma}$	=	vector of all $\gamma^{(i)}$ , $i \in \{1, \dots, M\}$
$\boldsymbol{\Gamma}^{\mathcal{G}}$	=	optimal activation set $\boldsymbol{\Gamma}$ under a control objective specification $\mathcal{G}$
$\boldsymbol{\Gamma}_{\text{path}}^{\mathcal{G}}$	=	linearly interpolated control path in the $\gamma$ -space, given an optimal activation set $\boldsymbol{\Gamma}^{\mathcal{G}}$
$\boldsymbol{\gamma}$	=	(note the boldface) vector of all activation parameters $\gamma_i$ , $i \in \{1, \dots, N\}$
$\delta_i$	=	functions of $R_1$ , $R_2$ , $\alpha_2$ , and $\nu$ appearing in the active filament formulae, $i \in \{0, 1, 2, 3\}$
$\epsilon_J$	=	positive hyperparameter defining the max. permissible value of $J^{\mathcal{G}}$ at $\boldsymbol{\Gamma}^{\mathcal{G}}$ for a sample to be valid
$\epsilon_f$	=	positive hyperparameter defining the max. permissible value of $f$ for a sample to be valid
$\zeta$	=	axial extension function for the filament
$\hat{\zeta}$	=	intrinsic version of $\zeta$

$\Theta$	= angle interval of $\theta$ values in which the activation $\gamma$ is non-zero
$\theta$	= polar angle in the annular cross section of the filament
$\theta_0$	= constant angular offset in the piecewise definition of $\gamma(\theta)$
$\hat{\mu}$	= predicted mean function in the GP
$\nu$	= Poisson's ratio of the filament
$\sigma$	= angular width of an active annular sector in the piecewise definition of $\gamma(\theta)$
$\hat{\sigma}$	= standard deviation function for the prediction in the GP
$\varphi$	= Fourier phase offset in the active filament formulae for $\hat{\mathbf{u}}$
$\chi$	= deformation map for the three-dimensional filament continuum
$\bullet^{(i)}$	= object $\bullet$ for the $i$ -th concentric tubular ring of the filament
$\bullet^{\text{new}}$	= object $\bullet$ newly evaluated at a given iteration of the Bayesian optimization
$\bullet^{\text{prior}}$	= object $\bullet$ corresponding to the set of priors for the Bayesian optimization
$\bullet^*$	= object $\bullet$ resulting from the Bayesian optimization ( $\mathcal{P}^*$ = best filament design found for a given $\mathcal{G}$ )
$\bullet^0$	= constant quantity $\bullet$ prescribed at the origin $Z = 0$
$ \bullet $	= cardinality of a set $\bullet$
$\otimes$	= tensor product operation

## 2. Introduction

A significant challenge in the field of robotics is the optimal control and design of soft actuators. While rigidly linked robotic arms are defined by a finite number of degrees of freedom, the motion of soft actuators involves, in principle, an infinite number of degrees of freedom [1], since every infinitesimal portion of the soft continuum can deform continuously in three-dimensional space. As a result, the quantitative modeling of soft actuators requires advanced mathematical constructions that are often computationally expensive. Currently, due to this great level of mechanical complexity, there is no robust, physics-informed, and generalizable control law for infinite-degree-of-freedom soft actuators [2]. Consequently, the challenges of soft actuator control, and the intricate mechanics of these structures both render the design of soft-robotic arms highly difficult [3].

To tackle the formidable challenge of soft actuator design, some researchers have looked to nature for inspiration in developing biomimetic designs of soft robotic arms [4]. This meta-level approach led to numerous prototypes mimicking the structure and mechanical principles of slender biological actuators such as the elephant trunk [5, 6, 7, 8], or the octopus arm [9, 10, 11, 12, 13, 14]. However, these biomimetic designs are largely based on qualitative decisions when translating the features of their biological counterparts into their respective engineering solutions. Further, past work relied primarily on empirical observations to guide the choices of the various design parameters. While this approach is interesting, it has not been an unmitigated success.

Another approach is to apply automated, quantitative optimization methodologies to identify most desirable soft-robotic designs [15] and state-of-the-art optimization methods have been implemented to derive optimal soft actuator geometries [16, 17], or actuation designs [18, 19] under various objective metrics. However, to date, soft-robotic actuator optimization lacks a formally generalized framework for determining actuator designs that maximize robotic adaptability and actuation versatility. This limitation exists partly because the most common methodologies for the design optimization of soft actuators rely mainly on computationally expensive models of actuator mechanics that utilize high-fidelity simulations to compute the objective function values. As a consequence, the high computational cost of most soft actuator models generally limits the evaluation of the actuator design to a singular robotic behavior paradigm—such as a particular

mode of deformation that the robotic arm should specialize in, or a desired target geometry of the actuator.

To address these limitations, we seek to bridge the qualitative bio-inspired design approach with a formalized, computationally efficient methodology for soft actuator design optimization under generalized control conditions. In particular, we apply a surrogate Bayesian optimization framework to optimize a biomimetic soft-robotic arm under a desired control objective. In principle, the deformation of an arbitrary soft actuator can be approximated computationally via multi-physics finite element analysis. However, a single execution of a finite-element simulation is a highly expensive operation and, as such, it is not a good candidate for a model-based approach for real-time soft actuator control. As such, we consider a special class of biomimetic actuator designs with embedded fibers, and model the actuator by applying a reduced-order active filament model [20], which ensures low computational cost for predicting the actuator deformation for a given control input. Most importantly, our approach seeks to identify efficiently fiber-based actuator designs that are optimal for arbitrary control objectives.

We proceed by first summarizing the active filament model [20] to quantify the physics of an arbitrarily designed fiber-based actuator. Then, we describe the optimization approach [21] to tackle the inverse problem of solving for the actuation needed to achieve a specific control objective, for a given actuator design. Finally, we outline, evaluate, and discuss the Bayesian optimization methodology to estimate optimal actuator designs under a specified control objective.

### 3. Active Filament Model

The active filament model uses the morphoelastic rod theory [22] to describe the mechanics of filaments with embedded active fiber fields in a reduced-order fashion [20]. In the following section, we briefly summarize the active filament theory as a prelude to the development of the optimization approach for identifying optimal fiber-based actuator designs.

#### 3.1. Generalized dimensional reduction

To reduce the computational cost of high-fidelity soft actuator modeling, we adopt a dimensional reduction of the actuator's three-dimensional filamentary continuum to a one-dimensional Kirchhoff rod [20, 23, 24, 25]. The resulting one-dimensional structure is defined by its centerline function  $\mathbf{r} : \mathbb{R} \rightarrow \mathbb{R}^3$ , and the director basis function  $\mathbf{D} = \{\mathbf{d}_1, \mathbf{d}_2, \mathbf{d}_3\}$ , where  $\mathbf{d}_i : \mathbb{R} \rightarrow \mathbb{R}^3$ . If  $Z$  denotes the material parameter of the filament, i.e., the arc length of the filament in the undeformed configuration, and  $L$  is its total length, then the centerline  $\mathbf{r}$  is a mapping from  $Z \in [0, L]$  to the one-dimensional space-curve shape of the deformed filament. Similarly,  $\mathbf{D}$  evaluated at  $Z$  defines an orthonormal basis that characterizes the local orientation of the deformed cross section at  $Z$ . By considering all  $Z \in [0, L]$ , the functions  $\mathbf{r}$  and  $\mathbf{D}$  together make up the dimensionally-reduced representation of the deformed filament.

The dimensional reduction results in a simplified form of the filament deformation  $\chi$  which maps the initial configuration  $\mathcal{B}$  to the current configuration  $\mathcal{B}_{\mathbb{A}}$ . In this reduced form, we write the deformation map in terms of  $\mathbf{r}$  and  $\mathbf{D}$  as

$$\chi(\mathbf{X}) = \mathbf{r}(Z) + \sum_{i=1}^3 \varepsilon a_i(\varepsilon R, \Theta, Z) \mathbf{d}_i(Z) \quad (1)$$

where  $\varepsilon$  is the small parameter of the thin rod geometry,  $a_i$  are the reactive strains that define the deformation of the cross section,  $\mathbf{X}$  is a point in  $\mathcal{B}$ , and  $\{R, \Theta, Z\}$  are the cylindrical coordinates of  $\mathbf{X}$ .

**Remark.** While we can equivalently express  $\chi(\mathbf{X})$  in any other coordinate system, it is most natural to write it in cylindrical coordinates due to the slender, tubular shape of the filamentary structure in its reference configuration.

To ensure the validity of the applied reduction, we further require that the cross sections  $\mathcal{S}(Z)$  satisfy

$$\forall Z : \int_{\mathcal{S}(Z)} EX dXdY = \int_{\mathcal{S}(Z)} EY dXdY = \int_{\mathcal{S}(Z)} EXY dXdY = 0, \quad (2)$$

where  $X$  and  $Y$  are the Cartesian coordinates in  $\mathbf{X} = (X, Y, Z) \in \mathcal{B}$ , and  $E$  is the Young's modulus of the filament material [20].

We express  $\mathbf{r}$  and  $\mathbf{D}$  most naturally in terms of the local (Darboux) curvature vector  $\mathbf{u} = \{u_1, u_2, u_3\}$  and the stretch  $\zeta$ , which are both functions of  $Z$ . The components  $u_1$  and  $u_2$  represent the local bending of the filament about the directors  $\mathbf{d}_1$  and  $\mathbf{d}_2$ , respectively, the component  $u_3$  corresponds to the local twist of the filament around  $\mathbf{d}_3$ , and  $\zeta$  describes the local stretch of the centerline  $\mathbf{r}$ . These functions are governed by the following system of ordinary differential equations that describes the kinematics of the filament:

$$\begin{aligned} \mathbf{r}'(Z) &= \zeta(Z)\mathbf{d}_3(Z), \\ \mathbf{d}'_i(Z) &= \zeta(Z)\mathbf{u}(Z) \times \mathbf{d}_i(Z), \end{aligned} \quad (3)$$

for  $i \in \{1, 2, 3\}$  [20]. For a given set of curvature and extension functions, we can compute the deformed configuration of the filament  $\{\mathbf{r}, \mathbf{D}\}$  by integrating (3) numerically.

**Remark.** The system of differential equations in (3) only has a closed-form analytical solution for special forms of the functions  $\mathbf{u}(Z)$  and  $\zeta(Z)$ . However, a generalized design of a fiber-based actuator does not produce these particular functions, so numerical integration of (3) is needed.

### 3.2. Special case of active filaments

The system of ordinary differential equations (3) is a geometric statement relating a filament shape to its curvatures. To obtain these curvatures, we assume that the elastic structure of interest is sufficiently slender. Then, the active filament theory [20] particularizes the filament geometry and characterizes the deformation as a result of fibrillar activation, which defines the expressions for the intrinsic curvature  $\hat{\mathbf{u}}$  and extension  $\hat{\zeta}$  that are analytically tractable.

In the active filament model, we specify a fiber field  $\mathbf{m} : \mathcal{B} \rightarrow \mathbb{R}^3$  at all points of the undeformed geometry  $\mathcal{B} \subset \mathbb{R}^3$ . For a tubular filament, we can construct an arbitrary fiber field in a cylindrical basis as

$$\mathbf{m} = (\sin \alpha \sin \beta) \mathbf{e}_R + (\sin \alpha \cos \beta) \mathbf{e}_\Theta + (\cos \alpha) \mathbf{e}_Z, \quad (4)$$

where  $\alpha$  and  $\beta$  are functions of the cylindrical coordinates  $\{R, \Theta, Z\}$ , with associated orthonormal basis vectors  $\{\mathbf{e}_R, \mathbf{e}_\Theta, \mathbf{e}_Z\}$ . The deformation then results from the *activation* of the fiber field defined by a tensor space  $\mathbf{G} : \mathcal{B} \rightarrow \mathbb{R}^3 \otimes \mathbb{R}^3$ , which is constructed such that one of its eigenvector fields is  $\mathbf{m}$ , and its two remaining eigenvector fields  $\mathbf{m}_\perp$  and  $\mathbf{m}'_\perp$  are orthonormal to  $\mathbf{m}$ . Assuming a small deviation of  $\mathbf{G}$  from  $\mathbf{1}$ , we define fibrillar activation such that the eigenvalues of  $\mathbf{G}$  corresponding to  $\mathbf{m}$ ,  $\mathbf{m}_\perp$  and  $\mathbf{m}'_\perp$  are

$$\delta = 1 + \varepsilon g(R, \Theta, Z), \quad \delta_\perp = \delta'_\perp = 1 - \varepsilon \nu g(R, \Theta, Z), \quad (5)$$

where  $\nu$  is the Poisson's ratio, and  $g$  is a scalar function of  $R$ ,  $\Theta$ , and  $Z$  [20]. As a result, the activation tensor becomes

$$\mathbf{G} = \mathbf{1} + \varepsilon g \begin{bmatrix} (1+\nu)\sin^2\alpha\sin^2\beta - \nu & (1+\nu)\sin^2\alpha\sin\beta\cos\beta & (1+\nu)\sin\alpha\cos\alpha\sin\beta \\ (1+\nu)\sin^2\alpha\sin\beta\cos\beta & -(1+\nu)\sin^2\alpha\sin^2\beta - \nu & (1+\nu)\sin\alpha\cos\alpha\cos\beta \\ (1+\nu)\sin\alpha\cos\alpha\sin\beta & (1+\nu)\sin\alpha\cos\alpha\cos\beta & \frac{1}{2}(1-\nu+(1+\nu)\cos 2\alpha) \end{bmatrix}. \quad (6)$$

This definition of  $\mathbf{G}$  explicitly defines the local contraction or extension of all fibers in the filament, with the Poisson effects captured by the determinant of  $\mathbf{G}$  [20]. To compute the deformation of the complete three-dimensional body, we adopt a multiplicative decomposition of the deformation gradient [23]:

$$\mathbf{F} = \text{Grad}\chi = \mathbf{A} \cdot \mathbf{G}, \quad (7)$$

where  $\chi$  is the deformation map,  $\mathbf{A}$  is the elastic part of the deformation gradient, and  $\mathbf{G}$  is the activation tensor [22]. Given the form of  $\chi$  in (1), we can write the deformation gradient as

$$\mathbf{F} = \begin{bmatrix} a_{1R} & \frac{1}{R}a_{1\Theta} & \varepsilon\zeta(u_2a_3 - u_3a_2) \\ a_{2R} & \frac{1}{R}a_{2\Theta} & \varepsilon\zeta(u_3a_1 - u_1a_3) \\ a_{3R} & \frac{1}{R}a_{3\Theta} & \zeta(1 + \varepsilon(u_1a_2 - u_2a_1)) \end{bmatrix}, \quad (8)$$

from which we can compute the elastic part  $\mathbf{A}$  for any specific activation tensor  $\mathbf{G}$  [20].

In general, from the deformation gradient  $\mathbf{F}$ , we can compute the filament's deformation upon arbitrary fibrillar activation by using the finite element method. However, such an approach is too computationally expensive for real-time filament control. Thus, we reduce the filament domain  $\mathcal{B}$  and its deformed configuration to their one-dimensional representations as described in Section 3.1, and re-express all other objects in terms of reduced-order quantities. We then write the total energy of the filament as

$$\mathcal{W} = \varepsilon^2 \int_0^L dZ \int_{\mathcal{S}(Z)} W(\mathbf{A})(\det \mathbf{G})R dR d\Theta, \quad (9)$$

where  $W$  is the strain energy density function. Noting that  $\mathbf{A} = \mathbf{F} \cdot \mathbf{G}^{-1}$ , we expand the energy  $\mathcal{W}$  up to the second order in the small parameter  $\varepsilon$ , assuming a quadratic strain energy density

$$W = \frac{1}{2} [\mu (\text{tr}(\mathbf{H} \cdot \mathbf{H}^T) + \text{tr}(\mathbf{H}^2)) + \lambda(\text{tr}(\mathbf{H}))^2], \quad (10)$$

where  $\mathbf{H} = \mathbf{A} - \mathbf{1}$ , and  $\mu$ ,  $\lambda$  are the Lamé parameters of the material [20]. Finally, we minimize the resulting energy functional  $\mathcal{W}$  up to  $\mathcal{O}(\varepsilon^4)$  over all admissible deformed configurations  $\{\mathbf{r}, \mathbf{D}\}$ . We express the terms in the resulting minimal energy in the standard form for Kirchhoff rods [23],

$$\mathcal{W} = \frac{1}{2} \int_0^L \left[ K_0(\zeta - \hat{\zeta})^2 + K_1(u_1 - \hat{u}_1)^2 + K_2(u_2 - \hat{u}_2)^2 + K_3(u_3 - \hat{u}_3)^2 \right] dZ, \quad (11)$$

to extract the stiffness coefficients  $K_0$ ,  $K_1$ ,  $K_2$ ,  $K_3$ , and the intrinsic curvature and extension functions  $\hat{u}_1$ ,  $\hat{u}_2$ ,  $\hat{u}_3$ , and  $\hat{\zeta}$ . Extracting these quantities yields the following analytical expressions [20]:

$$\hat{u}_1 = \frac{H_1}{K_1}, \quad \hat{u}_2 = -\frac{H_2}{K_2}, \quad \hat{u}_3 = \frac{H_3}{K_3}, \quad \hat{\zeta} = 1 + \frac{H_0}{K_0}, \quad (12)$$

where

$$\begin{aligned}
H_0 &= \frac{1}{2} \int_{\mathcal{S}(Z)} E(1 - \nu + (1 + \nu) \cos 2\alpha) g R dR d\Theta, \\
H_1 &= \frac{1}{2} \int_{\mathcal{S}(Z)} ER^2(1 - \nu + (1 + \nu) \cos 2\alpha) g \sin \Theta dR d\Theta, \\
H_2 &= \frac{1}{2} \int_{\mathcal{S}(Z)} ER^2(1 - \nu + (1 + \nu) \cos 2\alpha) g \cos \Theta dR d\Theta, \\
H_3 &= \frac{1}{2} \int_{\mathcal{S}(Z)} \frac{E}{\nu + 1} \left( g(\nu + 1) \sin(2\alpha) ((R^2 + \phi_\Theta) \cos \beta + R\phi_R \sin \beta) \right. \\
&\quad \left. - \frac{\omega_\Theta (\phi_\Theta + R^2)}{R} - R\omega_R \phi_R \right) dR d\Theta, \\
K_0 &= \int_{\mathcal{S}(Z)} ER dR d\Theta, \\
K_1 &= \int_{\mathcal{S}(Z)} ER^3 \sin^2 \Theta dR d\Theta, \\
K_2 &= \int_{\mathcal{S}(Z)} ER^3 \cos^2 \Theta dR d\Theta, \\
K_3 &= \int_{\mathcal{S}(Z)} \mu \left( R^3 + 2R\phi_\Theta + \frac{1}{R}\phi_\Theta^2 + R\phi_R^2 \right) dR d\Theta,
\end{aligned} \tag{13}$$

where the functions  $\phi$  and  $\omega$  satisfy

$$\begin{aligned}
\Delta\phi &= 0, \quad \mathbf{X} \in \mathcal{S}, \\
\mathbf{n} \cdot \text{Grad } \phi &= -R \mathbf{n} \cdot \mathbf{e}_\Theta, \quad \mathbf{X} \in \partial\mathcal{S}, \\
\Delta\omega &= -2R(1 + \nu) [\sin \alpha \cos \alpha (Rg_R \sin \beta + g_\Theta \cos \beta) \\
&\quad + g(-R\alpha_R \sin^2 \alpha \sin \beta + \alpha_\Theta \cos(2\alpha) \cos \beta) \\
&\quad + R\alpha_R \cos^2 \alpha \sin \beta - \beta_\Theta \sin \alpha \cos \alpha \sin \beta \\
&\quad + R\beta_R \sin \alpha \cos \alpha \cos \beta + \sin \alpha \cos \alpha \sin \beta)], \quad \mathbf{X} \in \mathcal{S}, \\
\mathbf{n} \cdot \text{Grad } \omega &= 0, \quad \mathbf{X} \in \partial\mathcal{S},
\end{aligned} \tag{14}$$

where  $\mathbf{n}$  is the outward normal of  $\partial\mathcal{S}$ ,  $g = g(R, \Theta, Z)$ , and  $\bullet_x$  denotes a derivative with respect to  $x$ . Most importantly, the primary result of the active filament model is the construction of an explicit relationship between the fibrillar activation and the deformation of the fiber-based filament.

In the most general case,  $\hat{\mathbf{u}}$  and  $\hat{\zeta}$  are functions of the fiber activation and the filament's geometry, despite being analytically explicit. Therefore, we adopt further simplifications of the filamentary structure [20], in which the tubular geometry of the filament consists of  $M$  concentric cylindrical rings  $\mathcal{R}^{(1)}, \dots, \mathcal{R}^{(M)}$ . The inner and outer radii  $R_1^{(i)}$  and  $R_2^{(i)}$ , respectively, define the geometry of the  $i$ -th ring, such that  $R_1^{(i)} = R_2^{(i-1)}$  to preserve domain continuity. Equivalently, we can represent the geometry of all rings in terms of independent parameters only, i.e., the inner radius  $R_1^{(1)}$  of the first ring, followed by  $M$  ring thickness values  $t^{(1)}, \dots, t^{(M)}$ . The specific form of the active filament theory considers a class of helical fiber fields embedded in each ring  $\mathcal{R}^{(i)}$  and defined via a helical angle  $\alpha_2^{(i)} \in (-\pi/2, \pi/2)$  [20]. Here,  $\alpha_2^{(i)} = 0$  corresponds to longitudinal fibers aligned with the long axis of the filament, while  $\alpha_2^{(i)} \neq 0$  represents a field of either right-handed

or left-handed helical fibers with  $\alpha_2^{(i)} > 0$  or  $\alpha_2^{(i)} < 0$ , respectively. With these assumptions, the expressions for the stress-free curvature and extension functions simplify to [20, 21]:

$$\begin{aligned}\hat{u}_1 &= -\frac{4}{3R_0^4} \sum_{i=1}^M A^{(i)} \delta_1^{(i)} \sin\left(\varphi^{(i)} - \frac{Z}{R_2^{(i)}} \tan \alpha_2^{(i)}\right), & \hat{u}_3 &= \frac{2}{R_0^4} \sum_{i=1}^M \delta_3^{(i)} a_0^{(i)}, \\ \hat{u}_2 &= -\frac{4}{3R_0^4} \sum_{i=1}^M A^{(i)} \delta_2^{(i)} \cos\left(\varphi^{(i)} - \frac{Z}{R_2^{(i)}} \tan \alpha_2^{(i)}\right), & \hat{\zeta} &= 1 + \frac{1}{2R_0^2} \sum_{i=1}^M a_0^{(i)} \delta_0^{(i)},\end{aligned}\quad (15)$$

where

$$a_0^{(i)} = \frac{1}{\pi} \int_0^{2\pi} \gamma^{(i)}(\theta) d\theta, \quad a_1^{(i)} = \frac{1}{\pi} \int_0^{2\pi} \gamma^{(i)}(\theta) \cos \theta d\theta, \quad b_1^{(i)} = \frac{1}{\pi} \int_0^{2\pi} \gamma^{(i)}(\theta) \sin \theta d\theta \quad (16)$$

are the first three Fourier coefficients of a prescribed fiber activation distribution  $\gamma^{(i)}(\theta)$  of the  $i$ -th ring, expressed in terms of the polar coordinate  $\theta$  in the annular cross section of  $\mathcal{R}^{(i)}$ . The set of activation distributions  $\Gamma(\theta) = \{\gamma^{(1)}(\theta), \dots, \gamma^{(M)}(\theta)\}$  fully defines the fibrillar activation—either contraction or extension—of the helical fiber fields in all  $M$  rings of the filament. The remaining quantities in (15) include the outer radius of the filament  $R_0 = R_2^{(M)}$ , the amplitude  $A^{(i)}$  and phase  $\varphi^{(i)}$  related via  $a_1^{(i)} = A^{(i)} \cos(\varphi^{(i)})$ ,  $b_1^{(i)} = -A^{(i)} \sin(\varphi^{(i)})$ , and the  $\delta_j^{(i)}$  factors,  $j \in \{0, 1, 2, 3\}$ , that are functions of  $R_1^{(i)}$ ,  $R_2^{(i)}$ ,  $\alpha_2^{(i)}$ , and the Poisson's ratio  $\nu^{(i)}$ .

**Remark.** The active filament model assumes that the activation results in changes of the purely intrinsic properties of the structure. As such, (15) does not account for the effect of external forces in predicting the resulting deformation. Nevertheless, if the filament is also subject to any external loading, we can use the intrinsic  $\hat{\mathbf{u}}$  and  $\hat{\zeta}$  in (15) to compute the curvatures  $\mathbf{u}$  and extension  $\zeta$  of the loaded filament, based on the classical equations of Kirchhoff rod mechanics [23].

### 3.3. Piecewise constant activation distribution

The form of the activation distribution  $\gamma^{(i)}(\theta)$  can, in principle, be an arbitrary function of  $\theta$ . In the context of slender biological actuators and soft-robotic arms, the fibers are often discrete and not distributed continuously. Thus, the form of  $\gamma(\theta)$  is restricted to piecewise constant functions [20, 21], in which annular sectors  $\Theta^{(i)} \times [R_1^{(i)}, R_2^{(i)}]$ , with non-zero values of  $\gamma^{(i)}$  indicate the presence of an activatable fiber over  $\theta \in \Theta^{(i)}$ , where  $\Theta^{(i)} \subset [0, 2\pi]$ , while all remaining annular sectors in the piecewise  $\gamma(\theta)$  are passive. Formally, we assume that the piecewise form of  $\gamma^{(i)}(\theta)$  is parametrized in terms of the number  $N^{(i)} \in \mathbb{Z}_+$  of active annular sectors with non-zero activation  $\gamma^{(i)}$ , the angular width  $\sigma^{(i)}$  of all active sectors, and the overall angular offset  $\theta_0^{(i)}$  of all active annular sectors. The angular distances between subsequent active sectors are determined by further enforcing  $N^{(i)}$ -fold rotational symmetry on  $\gamma^{(i)}(\theta)$ . Since the assumed form of  $\gamma^{(i)}(\theta)$  is piecewise constant, the value of  $\gamma^{(i)}$  remains constant within each individual active sector. As a result, it is natural to describe the piecewise constant activation  $\gamma^{(i)}(\theta)$  as a vector  $\boldsymbol{\gamma}^{(i)} \in \mathbb{R}^{N^{(i)}}$  of activation values for the respective  $N^{(i)}$  active sectors of the  $i$ -th ring. The fibrillar activation in the entire filament then becomes the vector  $\boldsymbol{\Gamma} = [\boldsymbol{\gamma}^{(1)}, \dots, \boldsymbol{\gamma}^{(M)}] \in \mathbb{R}^{\sum_i N^{(i)}}$  of activation values in all sectors across all  $M$  rings.

The curvature  $\mathbf{u}$  and extension  $\zeta$  are explicit functions of  $\boldsymbol{\Gamma}$ , the filament geometry parameter set  $\mathcal{D} = \{L, R_1^{(1)}, \mathbf{t}\}$ , the fiber architecture parameter set  $\mathcal{F} = \{\boldsymbol{\alpha}_2, \boldsymbol{\sigma}, \mathbf{N}, \boldsymbol{\theta}_0\}$ , and the mechanical properties of the filament  $\{\mathbf{E}, \boldsymbol{\nu}\}$ , where any boldface quantity  $\mathbf{X}$  denotes a vector  $[X^{(1)}, \dots, X^{(M)}]$ . We summarize the geometry  $\mathcal{D}$ , architecture  $\mathcal{F}$ , and the material properties  $\{\mathbf{E}, \boldsymbol{\nu}\}$  in the set  $\mathcal{P} = \mathcal{D} \cup \mathcal{F} \cup \{\mathbf{E}, \boldsymbol{\nu}\}$  to represent the set of all parameters describing the filament design. Fig. 1 summarizes the generalized design of a multi-ring active filament.

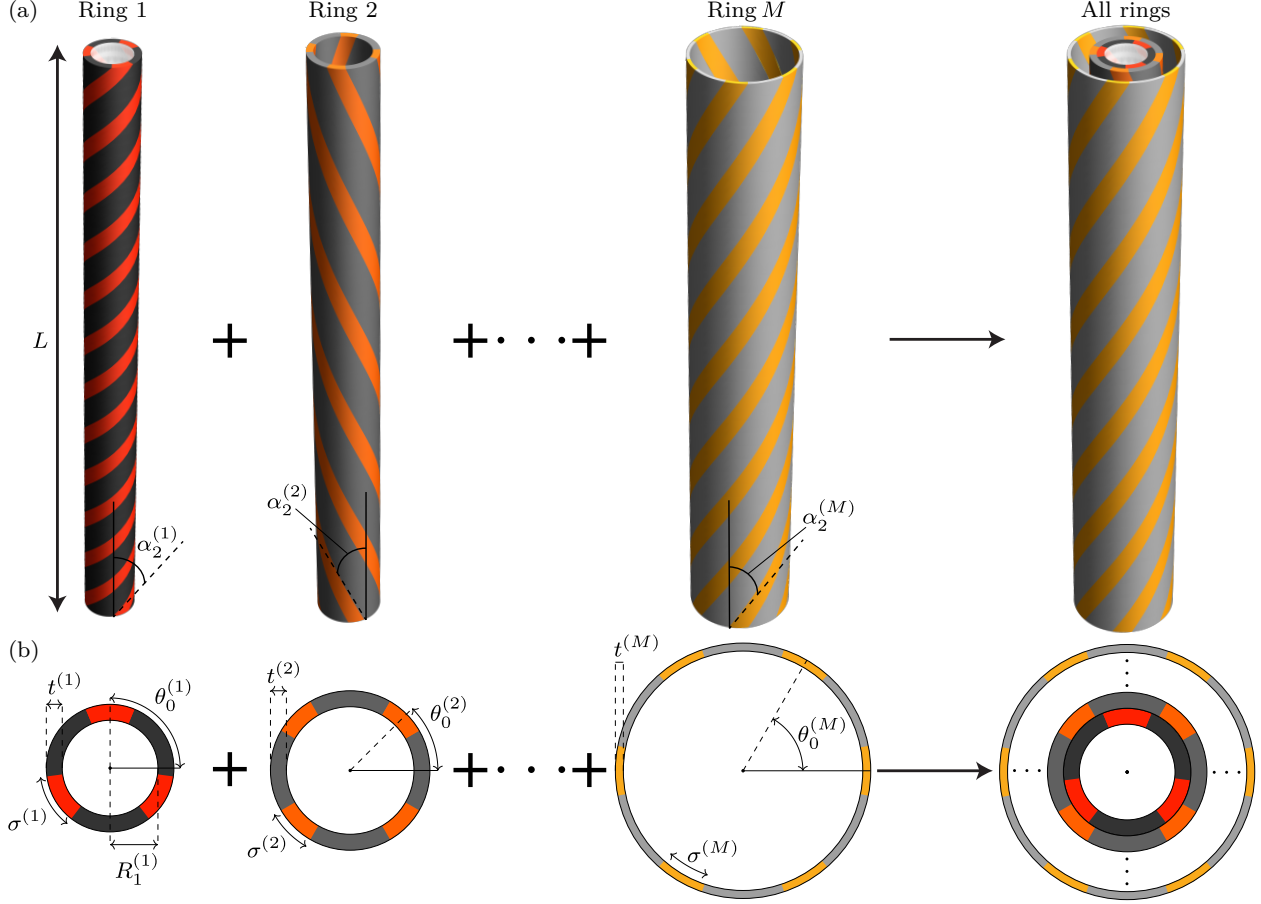


Figure 1: Generalized geometry of a multi-ring active filament with helical fibers and a piecewise uniform distribution of fibrillar activation. (a) Tubular geometry of individual rings  $\mathcal{R}^{(i)}$  with the respective helical fiber angles  $\alpha_2^{(i)}$ ,  $i = 1, \dots, M$ . (b) Cross sections of each cylindrical ring at  $Z = 0$ .

**Remark.** The dimensionality of the fiber activation vector  $\boldsymbol{\Gamma}$  depends on the set  $\mathcal{P}$ , since all  $\gamma^{(i)}$  are functions of the respective numbers of active sectors  $N^{(i)}$  in  $\mathbf{N}$ . Similarly, the number of independent parameters that control the deformation of the filament is also a function of  $\mathbf{N}$ .

The theory of active filaments defines the mapping from the fibrillar activation  $\boldsymbol{\Gamma}$  and the filament design  $\mathcal{P}$  to the curvature  $\mathbf{u}$  and extension  $\zeta$ . We denote this mapping with the shorthand notation  $\mathbb{A}(\boldsymbol{\Gamma}, \mathcal{P})$ . Passing the output  $\{\mathbf{u}, \zeta\}$  of  $\mathbb{A}(\boldsymbol{\Gamma}, \mathcal{P})$  to the system of differential equations in (3) and integrating yields the deformed configuration of the active filament  $\mathcal{B}_{\mathbb{A}}(Z; \boldsymbol{\Gamma}, \mathcal{P}) = \{\mathbf{r}(Z; \boldsymbol{\Gamma}, \mathcal{P}), \mathbf{D}(Z; \boldsymbol{\Gamma}, \mathcal{P})\}$ . The explicit relationship of  $\mathcal{B}_{\mathbb{A}}$  as a function of the fibrillar activation and the filament design is a starting point for the development of the optimization approach for fiber-based actuator design.

## 4. Optimization Approach

### 4.1. Actuator control: activation optimization

In this section, we briefly describe our actuator control approach [21] that sets the basis for the proposed filament design optimization method.

The active filament model  $\mathbb{A}$  tackles the forward problem of predicting the deformation  $\mathcal{B}_{\mathbb{A}}$  of an actuator, given the fiber activation input  $\boldsymbol{\Gamma}$ . Since the evaluation of  $\mathbb{A}$  for a given  $\boldsymbol{\Gamma}$  is inexpensive,

it is meaningful to formulate the basis of our control approach as an inverse problem of solving for the fiber activation  $\boldsymbol{\Gamma}$  required to achieve a target actuator deformation. We seek to construct an inverse mapping  $\mathbb{A}_{\boldsymbol{\Gamma}}^{-1}$  that maps the desired properties of a given deformation  $\mathcal{B}_{\mathbb{A}}$  to a fiber activation  $\boldsymbol{\Gamma}$ .

However, the numerical integration step required to obtain  $\mathcal{B}_{\mathbb{A}}$  with the specified properties from the output of  $\mathbb{A}$  renders the explicit derivation of the form of  $\mathbb{A}_{\boldsymbol{\Gamma}}^{-1}$  intractable. Instead, we approximate  $\mathbb{A}_{\boldsymbol{\Gamma}}^{-1}$  with an optimization problem over  $\boldsymbol{\Gamma} \in \mathcal{X}_{\boldsymbol{\Gamma}}$  defined by a control objective specification  $\mathcal{G}$ . The specification  $\mathcal{G}$  consists of a prescribed control goal  $\mathcal{G} = \mathcal{G}(\mathcal{B}_{\mathbb{A}})$ , the cost function  $J^{\mathcal{G}}(\mathcal{B}_{\mathbb{A}})$  associated with  $\mathcal{G}$ , and the set of activation constraints  $\mathcal{C}_{\boldsymbol{\Gamma}}$ . The control goal  $\mathcal{G}$  can be most naturally expressed as the target deformed configuration  $\mathcal{B}_{\mathbb{A}}^{\mathcal{G}}$  of the activated filament. In particular, let us define  $\mathcal{G}$  as a discrete mapping  $\mathcal{B}_{\mathbb{A}}(\mathcal{Z}) \rightarrow \mathcal{B}_{\mathbb{A}}^{\mathcal{G}}(\mathcal{S})$ , where  $\mathcal{Z}$  is a chosen set of material coordinates  $Z_i \in [0, L]$  at which  $\mathcal{B}_{\mathbb{A}}$  is to match  $\mathcal{B}_{\mathbb{A}}^{\mathcal{G}}$  evaluated at  $S_i \in \mathcal{S}$ , for  $i \in \{1, \dots, |\mathcal{Z}| = |\mathcal{S}|\}$ . Further, we take the cost function  $J^{\mathcal{G}}(\mathcal{B}_{\mathbb{A}})$  to be a weighted sum of the squared  $L_2$ -norm distances between the corresponding elements of  $\mathcal{B}_{\mathbb{A}}$  and  $\mathcal{B}_{\mathbb{A}}^{\mathcal{G}}$ , such that any deviation of the predicted configuration from the target configuration is penalized. Finally, the constraints  $c_{\boldsymbol{\Gamma}} \in \mathcal{C}_{\boldsymbol{\Gamma}}$  can be arbitrary functions of  $\boldsymbol{\Gamma}$ . In summary, the generalized control objective optimization problem under a specification  $\mathcal{G} = \{\mathcal{G}, J^{\mathcal{G}}, \mathcal{C}_{\boldsymbol{\Gamma}}\}$  is

$$\begin{aligned} & \underset{\boldsymbol{\Gamma}}{\text{minimize}} (J^{\mathcal{G}}(\mathcal{B}_{\mathbb{A}}(Z; \boldsymbol{\Gamma}, \mathcal{P}))), \quad \text{subject to } \mathcal{C}_{\boldsymbol{\Gamma}}, \\ & \text{where } \mathcal{G} : \mathcal{B}_{\mathbb{A}}(Z_i) \rightarrow \mathcal{B}_{\mathbb{A}}^{\mathcal{G}}(S_i), \forall i \in \{1, \dots, |\mathcal{Z}| = |\mathcal{S}|\}, \\ & \text{and } J^{\mathcal{G}}(\mathcal{B}_{\mathbb{A}}) = \sum_{i=1}^{|\mathcal{Z}|} \left( w_i \|\mathbf{r}(Z_i) - \mathbf{r}^{\mathcal{G}}(S_i)\|_2^2 + \sum_{j=1}^3 v_{ij} \|\mathbf{d}_j(Z_i) - \mathbf{d}_j^{\mathcal{G}}(S_i)\|_2^2 \right), \end{aligned} \tag{17}$$

with  $w_i, v_{ij} \geq 0$  defining the cost weights of all terms in  $J^{\mathcal{G}}$ .

We denote the minimizer of the above problem as  $\boldsymbol{\Gamma}^{\mathcal{G}}$ , under a specification  $\mathcal{G}$ . Algorithm 1 shows a pseudocode description of the solution of (17), for some arbitrary optimization scheme  $\mathcal{M}_{\boldsymbol{\Gamma}}$ . The implementation utilized in this work uses the Nelder-Mead simplex algorithm for  $\mathcal{M}_{\boldsymbol{\Gamma}}$  by default, but it can readily employ other schemes as well. We emphasize that this optimization problem assumes a constant parameter set  $\mathcal{P}$ , which is not the case for the developments in Sections 4.3 and 4.4.

**Remark.** Formally, the minimum of  $J^{\mathcal{G}}(\mathcal{B}_{\mathbb{A}})$  is 0 for a sufficiently versatile actuator design. However, most choices of the target configuration  $\mathcal{B}_{\mathbb{A}}^{\mathcal{G}}$  require a highly complex design to achieve  $\mathcal{G}$  exactly. In practice, after solving (17), a given actuator design will often only reach a configuration  $\mathcal{B}_{\mathbb{A}}$  with some finite deviation from  $\mathcal{B}_{\mathbb{A}}^{\mathcal{G}}$ , such that  $J^{\mathcal{G}}(\mathcal{B}_{\mathbb{A}}) > 0$ . Thus, the choice of the weights  $w_i, v_{ij}$  has a considerable impact on both the minimum  $J^{\mathcal{G}}(\mathcal{B}_{\mathbb{A}})$  and the minimizer  $\boldsymbol{\Gamma}^{\mathcal{G}}$ .

For the most general definition of  $\mathcal{G}$ , no single optimization scheme  $\mathcal{M}_{\boldsymbol{\Gamma}}$  utilized to solve (17) reaches a global minimum of  $J^{\mathcal{G}}$  robustly. Nonetheless, in this work, we evaluate our proposed filament design methodology under a relatively simplistic example of  $\mathcal{G}$ , for which the Nelder-Mead method proves to be a sufficiently effective choice for  $\mathcal{M}_{\boldsymbol{\Gamma}}$ . Specifically, we consider a class of control goals  $\mathcal{G}$  that prescribe a target endpoint position of the actuator. That is, the corresponding control objective specification is

$$\mathcal{G}_{\text{end}} = \{\mathcal{G}_{\text{end}}, J_{\text{end}}^{\mathcal{G}}, \mathcal{C}_{\boldsymbol{\Gamma}}\}, \tag{18}$$

where

$$\mathcal{G}_{\text{end}} : \mathbf{r}(L) \rightarrow \mathbf{r}_{\text{end}}^{\mathcal{G}}, \quad \text{and} \quad J_{\text{end}}^{\mathcal{G}}(\mathcal{B}_{\mathbb{A}}) = \|\mathbf{r}(L) - \mathbf{r}_{\text{end}}^{\mathcal{G}}\|_2^2, \tag{19}$$

---

**Algorithm 1** Quasi-static control objective optimization

---

**Require:**  $\mathcal{M}_\Gamma$ , ▷ Optimization scheme used in this algorithm; default = Nelder-Mead.  
 $\mathcal{G} = \{\mathcal{G}, \mathcal{C}_\Gamma, J^\mathcal{G}(\mathcal{B}_\mathbb{A}), \mathcal{Z}, \mathcal{S}\}$  ▷ Control objective specification  
 $\mathcal{P} = \mathcal{D} \cup \mathcal{F} \cup \{\mathbf{E}, \boldsymbol{\nu}\}$ , ▷  $\mathcal{P}$  = all filament properties,  $\mathcal{D}$  = filament geometry,  $\mathcal{F}$  = fiber architecture

where  $\mathcal{D} = \{L, R_1^{(1)}, \mathbf{t}\}$ ,  $\mathcal{F} = \{\boldsymbol{\alpha}_2, \boldsymbol{\sigma}, \mathbf{N}, \boldsymbol{\theta}_0\}$ ,  
with  $\mathbf{X} = \{X^{(1)}, \dots, X^{(M)}\}$ ,  $\forall X \in \{t, \alpha_2, \sigma, N, \theta_0, E, \nu\}$ ,  
and  $\forall i \in \{1, \dots, M\} : R_1^{(i)} \geq 0$ ,  $R_1^{(i+1)} = R_1^{(i)} + t^{(i)}$ ,  $t^{(i)} \geq 0$ ,  $\alpha_2^{(i)} \in (-\pi/2, \pi/2)$ ,  $\sigma^{(i)} \in [0, 2\pi/N^{(i)}]$ ,  $N^{(i)} \in \mathbb{Z}_+$ ,  $\theta_0^{(i)} \in [0, 2\pi)$ ,  $E^{(i)} \geq 0$ ,  $\nu^{(i)} \in [0, 1/2]$ , and  $L > 0$

$\hat{\zeta}(Z; \Gamma, \mathcal{P})$ ,  $\hat{\mathbf{u}}(Z; \Gamma, \mathcal{P}) \leftarrow \mathbb{A}(\Gamma; \mathcal{P})$  ▷ Active filament model  
 $\Gamma^\mathcal{G} \leftarrow \arg \min_{\Gamma} \left( J^\mathcal{G}(\mathcal{B}_\mathbb{A}(Z; \Gamma, \mathcal{P})) \text{ s.t. } \mathcal{C}_\Gamma, \text{ with scheme } \mathcal{M}_\Gamma \right)$   
where  $\mathcal{B}_\mathbb{A}(Z; \Gamma, \mathcal{P}) \leftarrow \text{Solve(Eq. (3), } \mathbf{r}|_{Z=0} = \mathbf{r}^0, \mathbf{d}_i|_{Z=0} = \mathbf{d}_i^0, i \in \{1, 2, 3\} \text{) } \right)$   
 $\Gamma_{\text{path}}^\mathcal{G} \leftarrow \gamma_0 \Gamma^\mathcal{G}$ ,  $\gamma_0 \in [0, 1]$  ▷ Optional control path output

---

for a desired endpoint position  $\mathbf{r}_{\text{end}}^\mathcal{G}$  of the actuator and a prescribed set of activation constraints. Examples of activation constraints include explicit restrictions on the activation parameters, i.e.,  $c_\Gamma = (\gamma_j^{(i)} \in [\gamma_{\min}, \gamma_{\max}], \forall i, j)$ ; maximum curvature magnitude constraints  $c_\Gamma = (\|\mathbf{u}(\Gamma, \mathcal{P})\|_2 \leq U_{\max}, U_{\max} > 0)$ ; or obstacle avoidance constraints  $c_\Gamma = (\mathbf{r}(Z; \Gamma, \mathcal{P}) \notin \mathcal{O}, \forall Z \in [0, L])$  for some obstacle region  $\mathcal{O} \subset \mathbb{R}^3$ .

An important assumption underlying the validity of applying the optimization-based form of  $\mathbb{A}_\Gamma^{-1}$  to soft actuator control is that the motion of the actuator is quasi-static. In particular, we assume that the time scale of transient effects due to fiber activation is long, i.e., no significant accelerations are present in the time-dependent deformation of the actuator. A potential quasi-static path of the actuator from its undeformed configuration to  $\mathcal{B}_\mathbb{A}^\mathcal{G}$  can then be constructed via linear interpolation of the optimal activation  $\Gamma^\mathcal{G}$ , i.e.  $\Gamma_{\text{path}}^\mathcal{G} = \gamma_0 \Gamma^\mathcal{G}$ , for  $\gamma_0 \in [0, 1]$ .

#### 4.2. Energy of activation

The quasi-static control approach relies on the optimization of a cost function  $J^\mathcal{G}$  based on a specification  $\mathcal{G}$ . To optimize the design of the geometry and fiber architecture of the actuator, we require another metric to optimize for. Here, we seek to optimize the actuator design under the control-optimal energetic cost of activation  $\mathcal{E}^\mathcal{G}$  to identify the design that is the most energetically efficient for a given control objective specification. The descriptor *control-optimal* refers to the fact that  $\mathcal{E}^\mathcal{G}$  is computed for the optimum  $\Gamma^\mathcal{G}$  obtained from the optimization problem in (17), and it is not an optimum with respect to  $\mathcal{P}$ .

The explicit form of the energetic cost of activation can take many forms, since activation itself is an abstract, dimensionless quantity that corresponds to fibrillar strains in the filament's fiber field. For a general, not necessarily piecewise form  $\Gamma^\mathcal{G}(\theta)$  of the activation distribution, we assume the following definition of the control-optimal activation energy,

$$\mathcal{E}^\mathcal{G}(\Gamma^\mathcal{G}) = \int_{\mathcal{A}} \Gamma^\mathcal{G}(\theta)^2 d\mathcal{A}, \quad (20)$$

where  $\mathcal{A}$  is the annular region of the transverse cross section of the filament. By construction,  $\Gamma(\theta)$  is not a function of  $Z$ , since its rotation around  $\mathbf{d}_3$  with respect to  $Z$  is implicitly captured in the  $\mathbb{A}$  formulae. As such, the integration over only the cross section provides a meaningful energy metric.

---

**Algorithm 2** Control-optimal energetic activation cost  $\mathcal{E}^{\mathcal{G}}$ , under control goal specification  $\mathcal{G}$ 


---

**Require:**  $\mathcal{G} = \{\mathcal{G}, \mathcal{C}_{\Gamma}, J^{\mathcal{G}}(\mathcal{B}_{\mathbb{A}}), \mathcal{Z}, \mathcal{S}\}$  ▷ Control objective specification  
 $\mathcal{P} = \mathcal{D} \cup \mathcal{F} \cup \{\mathbf{E}, \boldsymbol{\nu}\}$ , ▷ All filament parameters

$\boldsymbol{\Gamma}^{\mathcal{G}} \leftarrow \text{Algorithm 1}(\mathcal{G}, \mathcal{P})$  ▷ Solve the activation optimization problem  
 $\mathcal{E}^{\mathcal{G}} \leftarrow \frac{1}{2\pi} \sum_{i=1}^M \left( (R_2^{(i)})^2 - (R_1^{(i)})^2 \right) \sigma^{(i)} \left\| \boldsymbol{\gamma}^{\mathcal{G}(i)} \right\|_2^2$  ▷ Energetic cost of activation

---

Assuming the piecewise constant activation distribution  $\boldsymbol{\Gamma}$  from Section 3.3, we can equivalently write the energy in (20) as

$$\mathcal{E}^{\mathcal{G}}(\boldsymbol{\Gamma}^{\mathcal{G}}) = \frac{1}{2\pi} \sum_{i=1}^M \left( (R_2^{(i)})^2 - (R_1^{(i)})^2 \right) \sigma^{(i)} \left\| \boldsymbol{\gamma}^{\mathcal{G}(i)} \right\|_2^2, \quad (21)$$

which enables cheap computation of the control-optimal activation cost. Algorithm 2 provides a schematic implementation of the chosen activation energy metric.

**Remark.** Since  $\mathcal{E}^{\mathcal{G}}$  is a function of  $\mathcal{P}$  and the minimizer of the optimization problem (17), it can be equivalently expressed as a function of  $\mathcal{G}$  and  $\mathcal{P}$  as

$$\mathcal{E}^{\mathcal{G}} = \mathcal{E}^{\mathcal{G}} \left( \arg \min_{\boldsymbol{\Gamma}} (J^{\mathcal{G}}(\mathcal{B}_{\mathbb{A}}(Z; \boldsymbol{\Gamma}, \mathcal{P})), \text{ s.t. } \mathcal{C}_{\Gamma} \right) \Leftrightarrow \mathcal{E}^{\mathcal{G}} = \mathcal{E}^{\mathcal{G}}(\mathcal{G}, \mathcal{P}), \quad (22)$$

which we adopt in our implementation.

#### 4.3. Automated actuator design

The main goal of this work is to formulate a methodology for identifying optimal fiber-based actuator designs under a prescribed control objective. Our hypothesis is that a potentially viable approach for this optimization goal is to minimize the control-optimal energetic cost of activation  $\mathcal{E}^{\mathcal{G}}$  over the space  $\mathcal{X}_{\mathcal{P}}$  of all feasible actuator designs  $\mathcal{P}$ , for a specific control objective specification  $\mathcal{G}$ . In its most general form, this optimization problem becomes

$$\begin{aligned} & \underset{\mathcal{P}}{\text{minimize}} \left( \mathcal{E}^{\mathcal{G}}(\mathcal{G}, \mathcal{P}) \right), \\ & \text{subject to } \mathcal{P} \in \mathcal{X}_{\mathcal{P}}. \end{aligned} \quad (23)$$

Importantly, (23) is a nested optimization problem, for which every evaluation of  $\mathcal{E}^{\mathcal{G}}$  requires a complete solution of the optimization problem in (17) for a given  $\mathcal{P}$ , and the prescribed  $\mathcal{G}$ . In the following, we evaluate the validity of the approach defined by (23) and assume the simplified form of  $\mathcal{G}$  in (18), in which the control goal is for the actuator's endpoint to reach a prescribed target position. Algorithm 1 outlines the definition of the largest permissible feasible set  $\mathcal{X}_{\mathcal{P}}$  in its input requirements. In practice, we introduce further restrictions on  $\mathcal{P}$  to improve the optimization performance, and avoid regions of  $\mathcal{P}$  that result in a significant increase in computational cost.

#### 4.4. Bayesian optimization

Since every evaluation of  $\mathcal{E}^{\mathcal{G}}$  involves solving an entire optimization problem, function evaluations in (23) are computationally expensive. Preliminary testing revealed that solving (23) directly by using an optimization method such as the Nelder-Mead simplex method or population-based

schemes results in either no significant improvement of the objective value over any feasible number of function evaluations, or premature convergence to a local optimum. The elevated computational cost motivates the construction of a surrogate model to estimate  $\mathcal{E}^{\mathcal{G}}$  and compute an approximate solution of (23) in a feasible time. In particular, we chose a Gaussian process as a probabilistic surrogate model for the purposes of Bayesian optimization. The Gaussian process object is defined as

$$\text{GP} = \text{GP}(m, k_{\text{GP}}; H), \quad (24)$$

where  $m$  is the mean function,  $k_{\text{GP}}$  is the kernel, and  $H = \{(x_1, h(x_1)), (x_2, h(x_2)), \dots\}$  is the function evaluation history for a function  $h : D \rightarrow \mathbb{R}$  approximated by the Gaussian process, for a given design space  $D$ . The Gaussian process used in this work assumes a zero mean,  $m = 0$ , and a Matérn kernel of the form

$$k_{\text{GP}}(x, x') = \frac{1}{2^{\tilde{\nu}-1}\tilde{\Gamma}(\tilde{\nu})} \left( \frac{2\sqrt{\tilde{\nu}}}{\vartheta} \|x - x'\|_2 \right)^{\tilde{\nu}} K_{\tilde{\nu}} \left( \frac{2\sqrt{\tilde{\nu}}}{\vartheta} \|x - x'\|_2 \right), \quad (25)$$

where  $\tilde{\Gamma}$  is the Gamma function and  $K_{\tilde{\nu}}$  is the modified Bessel function of the second kind [26]. We selected the Matérn kernel over the classical squared exponential kernel, as it is more parametrically flexible [27] and could capture more intricate features of  $\mathcal{E}^{\mathcal{G}}$ . For machine learning applications, Matérn kernels with  $\tilde{\nu} = 3/2$  and  $\tilde{\nu} = 5/2$  are most preferable [28]. Ultimately, the value  $\tilde{\nu} = 5/2$  was ultimately selected, as it yielded better performance in preliminary testing.

Before we can use the surrogate Gaussian process for Bayesian optimization, we need to augment algorithmically the mathematical description of the control-optimal activation energy  $\mathcal{E}^{\mathcal{G}}$  to ensure meaningful optimization results. The primary reason for a more careful treatment of the  $\mathcal{E}^{\mathcal{G}}$  evaluation algorithm is that Algorithm 1 is not guaranteed to converge to a global minimum, and, even if it does find a global minimizer  $\boldsymbol{\Gamma}^{\mathcal{G}}$ , the value of  $J^{\mathcal{G}}$  at that global minimum could be positive for some  $\mathcal{G}$  and  $\mathcal{P}$ . This occurs whenever a given actuator design  $\mathcal{P}$  cannot achieve  $\mathcal{G}$  for any activation  $\boldsymbol{\Gamma} \in \mathcal{X}_{\boldsymbol{\Gamma}}$ . As a result, whenever  $\boldsymbol{\Gamma}^{\mathcal{G}}$  results in a small  $\mathcal{E}^{\mathcal{G}}$  and  $J^{\mathcal{G}} > 0$ , optimizing  $\mathcal{E}^{\mathcal{G}}$  according to (23) would yield misleading optimization results, because the small energetic activation cost would correspond to an actuator with poor control capabilities for the prescribed control objective.

The described behavior leads to the first, simple augmentation of  $\mathcal{E}^{\mathcal{G}}$ . We add a Boolean flag output  $\text{GC} = (J^{\mathcal{G}} \leq \epsilon_J)$  that is **true** if the computed optimal activation  $\boldsymbol{\Gamma}^{\mathcal{G}}$  results in satisfactory control, and false otherwise. We measure the quality of the control result by using a small hyperparameter threshold  $\epsilon_J > 0$ . This additional output enables more flexibility in the design of the Bayesian optimization method, as it effectively allows monitoring the actuator control quality at each step of the objective minimization.

The second modification of  $\mathcal{E}^{\mathcal{G}}$  is meant purely to increase the computational robustness of the Bayesian optimization process. In particular, for a machine with  $n_{\text{core}}$  cores,  $\mathcal{E}^{\mathcal{G}}$  is evaluated  $n_{\text{core}}$  times in parallel, with several randomized modifications applied to each evaluation to increase the success rate of the optimization scheme  $\mathcal{M}_{\boldsymbol{\Gamma}}$  in solving (17) globally. On all cores, we initialize the seed in  $\mathcal{M}_{\boldsymbol{\Gamma}}$  with a random value, assuming that  $\mathcal{M}_{\boldsymbol{\Gamma}}$  incorporates stochasticity. We determine the initial points passed to  $\mathcal{M}_{\boldsymbol{\Gamma}}$  based on the set of available priors  $H^{\text{prior}} = \{(\mathcal{P}_1^{\text{prior}}, f_1^{\text{prior}}), \dots, (\mathcal{P}_{n_{\text{prior}}}^{\text{prior}}, f_{n_{\text{prior}}}^{\text{prior}})\}$ . Concretely, we first compute a set of  $n_{\text{init}}$  points  $\mathcal{P}^{\text{prior}}$  in  $H^{\text{prior}}$  closest to the current  $\mathcal{P}$  in  $L_2$ -norm, and denote it as  $\{\mathcal{P}_1^{\text{near}}, \dots, \mathcal{P}_{n_{\text{init}}}^{\text{near}}\}$ . Then, on one of the cores, we extract the set of all optimal  $\boldsymbol{\Gamma}_i^{\mathcal{G}}$  corresponding to the respective  $\mathcal{P}_i^{\text{near}}$ ,  $i \in \{1, \dots, n_{\text{init}}\}$  and use it as the set of initial points for  $\mathcal{M}_{\boldsymbol{\Gamma}}$ , e.g., for the initialization of the simplex if we choose the Nelder-Mead simplex method for  $\mathcal{M}_{\boldsymbol{\Gamma}}$ .

---

**Algorithm 3** Objective  $f$ , under control goal specification  $\mathcal{G}$ 


---

**Require:**  $\mathcal{G} = \{\mathcal{G}, \mathcal{C}_\Gamma, J^\mathcal{G}(\mathcal{B}_\mathbb{A}), \mathcal{Z}, \mathcal{S}\}$  ▷ Control objective specification  
 $\mathcal{P} = \mathcal{D} \cup \mathcal{F} \cup \{\mathbf{E}, \boldsymbol{\nu}\}$ , ▷ All filament parameters  
 $O = \{\epsilon_J, n_{\text{init}}, \mathbf{Z}_{\min}, \mathbf{Z}_{\max}\}$ , ▷ Auxiliary optimization hyperparameters  
**is\_prior** ▷ Flag indicating whether the input is a prior or not

```

if is_prior then
     $\boldsymbol{\Gamma}^\mathcal{G}, \mathcal{E}^\mathcal{G} \leftarrow \text{Algorithm 2}(\mathcal{G}, \mathcal{P})$ 
else
    Require:  $\{\mathcal{P}_1^{\text{prior}}, \dots, \mathcal{P}_{n_{\text{prior}}}^{\text{prior}}\}$  ▷ Prior design points
     $\{\mathcal{P}_1^{\text{near}}, \dots, \mathcal{P}_{n_{\text{init}}}^{\text{near}}\} \leftarrow n_{\text{init}}$  design points in  $\{\mathcal{P}_1^{\text{prior}}, \dots, \mathcal{P}_{n_{\text{prior}}}^{\text{prior}}\}$  closest to  $\mathcal{P}$  in  $L_2$ -norm
        that satisfy the  $N^{(i)}$  matching condition
     $\{\boldsymbol{\Gamma}_1^\mathcal{G}, \dots, \boldsymbol{\Gamma}_{n_{\text{init}}}^\mathcal{G}\} \leftarrow \boldsymbol{\Gamma}^\mathcal{G}$  optimal activation points corresponding to the
         $\{\mathcal{P}_1^{\text{near}}, \dots, \mathcal{P}_{n_{\text{init}}}^{\text{near}}\}$  priors
    for  $i \leftarrow 1$  to  $n_{\text{core}}$  do ▷ Evaluate the for-loop body on each CPU core in parallel
         $S \leftarrow$  Randomized seed for activation optimization
        if  $i \geq 2$  then
            for  $j \leftarrow 1$  to  $n_{\text{init}}$  do
                 $\mathbf{Z} \sim \mathcal{U}(\mathbf{Z}_{\min}, \mathbf{Z}_{\max})$  ▷ Uniform sampling from  $[\mathbf{Z}_{\min}, \mathbf{Z}_{\max}]$ ,
                 $\mathbf{Z} = (\mathbf{z}^{(1)}, \dots, \mathbf{z}^{(M)}), \mathbf{z}^{(k)} \in \mathbb{R}^{N^{(k)}}$ 
                 $\boldsymbol{\Gamma}_j^\mathcal{G} \leftarrow \boldsymbol{\Gamma}_j^\mathcal{G} + \mathbf{Z}$ 
            end for
        end if
         $\boldsymbol{\Gamma}_{[i]}^\mathcal{G}, \mathcal{E}_{[i]}^\mathcal{G} \leftarrow \text{Algorithm 2}(\mathcal{G}, \mathcal{P})$ , with seed  $S$ , and initial points  $\{\boldsymbol{\Gamma}_1^\mathcal{G}, \dots, \boldsymbol{\Gamma}_{n_{\text{init}}}^\mathcal{G}\}$ 
    end for
     $I \leftarrow \arg \min_{i \in \{1, \dots, n_{\text{core}}\}} (J^\mathcal{G}(\mathcal{B}_\mathbb{A}(Z; \boldsymbol{\Gamma}_{[I]}^\mathcal{G}, \mathcal{P}))$ 
     $\boldsymbol{\Gamma}^\mathcal{G}, \mathcal{E}^\mathcal{G} \leftarrow \boldsymbol{\Gamma}_{[I]}^\mathcal{G}, \mathcal{E}_{[I]}^\mathcal{G}$ 
end if
 $f \leftarrow \mathcal{E}^\mathcal{G}$ 
 $\text{GC} \leftarrow (J^\mathcal{G}(\mathcal{B}_\mathbb{A}(Z; \boldsymbol{\Gamma}^\mathcal{G}, \mathcal{P})) \leq \epsilon_J)$  ▷ Flag indicating whether  $\boldsymbol{\Gamma}^\mathcal{G}$  results in satisfactory control

```

---

**Remark.** Importantly, for a given input  $\mathcal{P}$ , the  $L_2$ -norm distances in  $\mathcal{P}$ -space are only valid if all  $N^{(i)}$  in  $\mathcal{P}$  match with all  $N^{(i)}$  in the priors used for comparison, since the dimensionality of the corresponding prior  $\boldsymbol{\Gamma}$  vectors has to match the dimensionality of  $\boldsymbol{\Gamma}$  defined by  $\mathcal{P}$ . Priors for which this matching condition is not met are not used in the search for closest points. If no priors meet the condition, then we randomize the  $\boldsymbol{\Gamma}$  initialization in  $\mathcal{M}_\Gamma$ .

Finally, on all remaining cores, we perturb the extracted initial point candidates  $\boldsymbol{\Gamma}_i^\mathcal{G}$  by a random perturbation  $\mathbf{Z}$  sampled from a continuous uniform distribution  $\mathcal{U}(\mathbf{Z}_{\min}, \mathbf{Z}_{\max})$ , where  $\mathbf{Z}_{\min}$  and  $\mathbf{Z}_{\max}$  are the sets of minimum and maximum bounds on the admissible perturbations for parameters in  $\boldsymbol{\Gamma}$ . Introducing these parallelized modifications into  $\mathcal{E}^\mathcal{G}$  increases the chance to find a global optimum on at least one of the cores, while preserving computational performance.

We compile these augmentations of  $\mathcal{E}^\mathcal{G}$  into a new objective function  $f(\mathcal{G}, \mathcal{P})$  implemented in Algorithm 3. We optimize the function  $f$  using Bayesian optimization, according to the augmented

optimization problem

$$\begin{aligned} & \text{Bay minimize}_{\mathcal{P}} (f(\mathcal{G}, \mathcal{P})), \\ & \text{subject to } \mathcal{P} \in \mathcal{X}_{\mathcal{P}}, \end{aligned} \tag{26}$$

where the prefix ‘‘Bay’’ emphasizes that the minimization of  $f$  occurs in a Bayesian sense, using the Gaussian process in (24), (25).

The Bayesian optimization approach chooses the evaluation points  $\mathcal{P}$  heuristically by maximizing the expected improvement of  $f$  according to the surrogate Gaussian process, based on the current evaluation history  $H$ . Specifically, each step of the Bayesian optimization involves solving the following maximization problem,

$$\begin{aligned} & \text{maximize}_{\mathcal{P}} (\mathbb{E}[\text{Imp}(f(\mathcal{G}, \mathcal{P}))]), \quad \text{subject to } \mathcal{P} \in \mathcal{X}_{\mathcal{P}}, \\ & \text{where } \text{Imp}(f(\mathcal{G}, \mathcal{P})) = \begin{cases} f_{\min} - f(\mathcal{G}, \mathcal{P}), & \text{for } f < f_{\min}, \\ 0, & \text{otherwise,} \end{cases} \end{aligned} \tag{27}$$

and  $f_{\min}$  is the minimum of  $f$  among the points  $\{\mathcal{P}, f\}$  in the current evaluation history  $H$ . We solve (27) using a chosen optimization scheme  $\mathcal{M}_{\mathbb{E}}$ .

**Remark.** We emphasize that the maximization in (27) does not involve any evaluations of  $f$  since the expectation  $\mathbb{E}[\text{Imp}(f)]$  is only a function of  $f_{\min}$ , and the predicted mean  $\hat{\mu}$  and standard deviation  $\hat{\sigma}$  of the Gaussian process. This property of maximization problem is crucial since the solution of (27) provides the next evaluation point for  $f$ , so it cannot involve the computation of  $f$ .

Evaluating the objective function at the maximizer  $\mathcal{P}^{\text{new}}$  of (27) produces the new evaluation point  $\{\mathcal{P}^{\text{new}}, f(\mathcal{G}, \mathcal{P}^{\text{new}})\}$ . If  $\text{GC} = \text{true}$ , i.e., the actuator exhibits satisfactory control, and if  $f \leq \epsilon_f$  for some hyperparameter  $\epsilon_f > 0$ , then we add the new evaluation point to the evaluation history  $H$ . The  $f \leq \epsilon_f$  condition mitigates the erratic multi-branched functional characteristics of  $\mathcal{E}^{\mathcal{G}}$ , see Section 5.2. If any of these two conditions is not satisfied, we restart the maximization in (27) with a randomized initialization for  $\mathcal{M}_{\mathbb{E}}$ . We permit a maximum of  $N_{\text{res}}$  such restarts. Subsequently, we re-train the parameters of the Gaussian process for the new evaluation history  $H$ , and the Bayesian optimization continues until a maximum number of steps  $K$  is reached. We train the Gaussian process by maximizing the likelihood of  $H$  with respect to the parameters of the Gaussian process using the simulated annealing algorithm. Algorithm 4 summarizes the utilized Bayesian optimization approach. Fig. 2 synthesizes the nested computational structure of the methodology.

**Remark.** Even though the number of active sectors in the  $i$ -th ring of the filament,  $N^{(i)} \in \mathcal{P}$ , is only defined over positive integers, we generalize the input to the Gaussian process to any vectors in  $\mathbb{R}^{|\mathcal{P}|M}$  to improve robustness, as compared to using a Gaussian process with a mixed input type. To accommodate the real-valued elements  $N^{(i)}$  in the result  $\mathcal{P}$  of maximizing the expectation in (27), we round the values  $N^{(i)}$  to the nearest integers for every evaluation of  $f$ .

Since the evaluations of  $f$  are expensive, it is important that the sampling plan used for the prior initialization of  $H$  exhibits low discrepancy. As such, we construct the sampling plan for  $H^{\text{prior}}$  using a  $|\mathcal{P}|$ -dimensional Sobol quasi-random sequence [29], with  $\tilde{n}_{\text{prior}}$  samples over the feasible set  $\mathcal{X}_{\mathcal{P}}$ . We initialize the prior evaluation history  $H^{\text{prior}} = \{(\mathcal{P}_1^{\text{prior}}, f_1^{\text{prior}}), \dots, (\mathcal{P}_{\tilde{n}_{\text{prior}}}^{\text{prior}}, f_{\tilde{n}_{\text{prior}}}^{\text{prior}})\}$  according to the obtained low-discrepancy sampling plan. Before passing it as one of the inputs to Algorithm 4, we further process it by discarding all points in  $H^{\text{prior}}$  for which  $f(\mathcal{G}, \mathcal{P}^{\text{prior}}) > \epsilon_f$ , with  $\epsilon_f$  defined as in Algorithm 4, or for which the corresponding  $\mathbf{F}^{\mathcal{G}}$  results in  $J^{\mathcal{G}} > \epsilon_J$ , with  $\epsilon_J$

---

**Algorithm 4** Bayesian optimization of  $f$  (Bay min)

---

**Require:**  $\mathcal{M}_{\mathbb{E}}$ , ▷ Optimization scheme for max. expected imp. maximization  
 $f$  ▷  $f$  defined by **Algorithm 3**  
 $\mathcal{X}_{\mathcal{P}}$ , ▷  $\mathcal{X}_{\mathcal{P}} =$  Feasible set of  $\mathcal{P}$   
 $O = \{\epsilon_J, \epsilon_f, n_{\text{init}}, \mathbf{Z}_{\text{min}}, \mathbf{Z}_{\text{max}}\}$ , ▷ Auxiliary optimization hyperparameters  
 $\mathcal{G} = \{\mathcal{G}, \mathcal{C}_{\Gamma}, J^{\mathcal{G}}(\mathcal{B}_{\mathbb{A}}), \mathcal{Z}, \mathcal{S}\}$  ▷ Control objective specification  
 $H^{\text{prior}}$  ▷ Prior evaluation history  
 $K \geq 1$  ▷ Number of iterations in Bayesian optimization  
 $N_{\text{res}}$  ▷ Maximum permissible number of restarts for  $\mathcal{M}_{\mathbb{E}}$

$k_{\text{GP}}(x, x') \leftarrow \frac{1}{2^{\tilde{\nu}-1}\tilde{\Gamma}(\tilde{\nu})} \left( \frac{2\sqrt{\tilde{\nu}}}{\vartheta} \|x - x'\|_2 \right)^{\tilde{\nu}} K_{\tilde{\nu}} \left( \frac{2\sqrt{\tilde{\nu}}}{\vartheta} \|x - x'\|_2 \right)$

$\text{GP} \leftarrow \text{GP}(0, k_{\text{GP}}; H^{\text{prior}})$  ▷ Initialize a 0-mean GP with kernel  $k_{\text{GP}}$ , and the given priors  
 $H \leftarrow H^{\text{prior}}$  ▷ Evaluation history

$f_{\text{min}} \leftarrow \text{minimum } f \text{ in } H$

**for**  $k \leftarrow 1$  to  $K$  **do**

**for**  $l \leftarrow 1$  to  $N_{\text{res}}$  **do**

$\mathcal{P}^{\text{new}} \leftarrow \arg \max_{\mathcal{P}} \left( \mathbb{E}[\text{Imp}(\text{Algorithm 3}(\mathcal{G}, \mathcal{P}; O))], \text{ with } \mathcal{P} \in \mathcal{X}_{\mathcal{P}},$   
▷ Maximize expected improvement  
            for  $f_{\text{min}}$ , and  $\hat{\mu}, \hat{\sigma}$  in GP, given  $H$ , with scheme  $\mathcal{M}_{\mathbb{E}}$   
                ▷ Maximize expected improvement

$f^{\text{new}}, \text{GC} \leftarrow \text{Algorithm 3}(\mathcal{G}, \mathcal{P}^{\text{new}}; O)$   
        **if** GC **and**  $f^{\text{new}} \leq \epsilon_f$  **then**  
            **break**  
        **else**  
            Randomize the initialization of  $\mathcal{M}_{\mathbb{E}}$  for next iteration  
        **end if**  
    **end for**  
    **if**  $f^{\text{new}} < f_{\text{min}}$  **then**  $f_{\text{min}} \leftarrow f^{\text{new}}$  **end if**  
     $H \leftarrow H \cup \{(\mathcal{P}^{\text{new}}, f^{\text{new}})\}$   
     $\text{GP} \leftarrow \text{Fit}(\text{GP}(0, k_{\text{GP}}; H))$  ▷ Re-train the GP by maximizing the likelihood of the updated  $H$

**end for**

$\mathcal{P}^* \leftarrow \mathcal{P}$  corresponding to minimum  $f$  from all  $(\mathcal{P}, f) \in H$

---

defined as in Algorithm 3. Similar to the approach within the Bayesian optimization itself, this prior processing step removes all samples with significantly larger control-optimal energies  $\mathcal{E}^{\mathcal{G}}$ , and all samples for which the solution of the activation optimization problem (17) results in poor actuator control. Finally, we select a prescribed number  $n_{\text{prior}} < \tilde{n}_{\text{prior}}$  of samples from the post-processed set  $H^{\text{prior}}$  to eliminate randomness from the number of priors provided to the Gaussian process.

**Remark.** Importantly, the original number of sampling plan sites  $\tilde{n}_{\text{prior}}$  needs to be sufficiently large, so that the sample discarding process does not eliminate more than  $\tilde{n}_{\text{prior}} - n_{\text{prior}}$  samples, which would ultimately result in  $H^{\text{prior}} = \emptyset$ . At the same time,  $n_{\text{prior}}$  should also be large enough, so that the prior surrogate model of  $\mathcal{E}^{\mathcal{G}}$  guides the optimization effectively.

Algorithm 5 describes the complete approach for Bayesian optimization of all parameters that define the fiber-based actuator under a prescribed control objective specification.

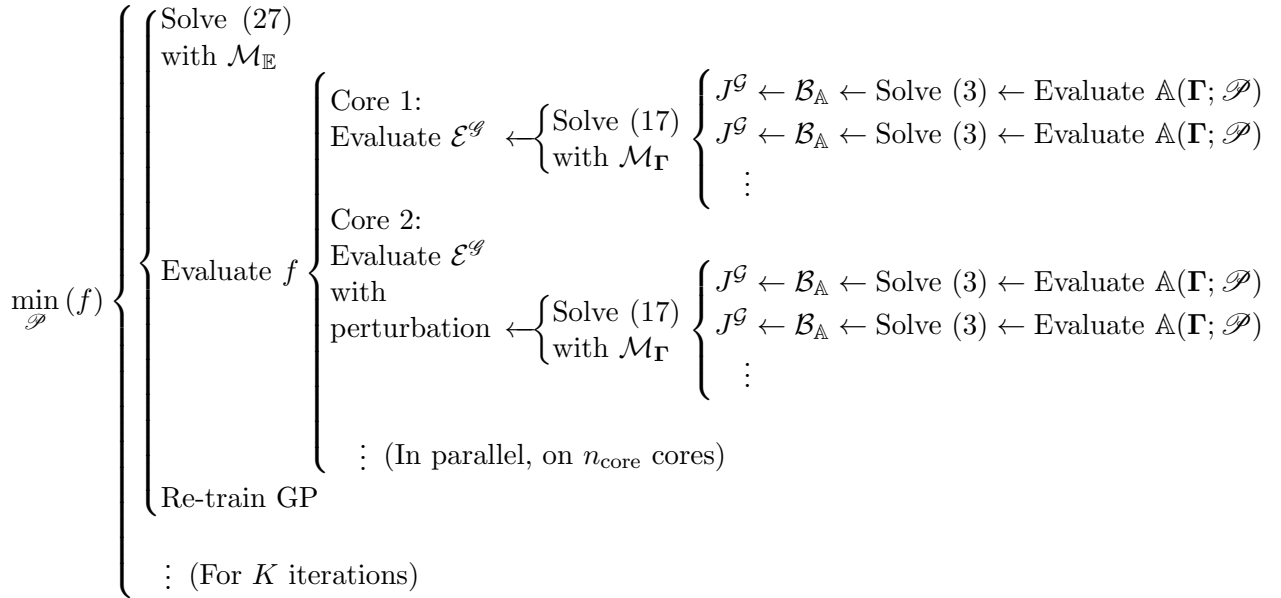


Figure 2: The nested computational structure of the minimization methodology utilized to optimize the filament design. Only the most major components of the implementation are depicted in the above schematic; refer to Algorithms 1-6 for the details of the implementation.

---

**Algorithm 5** Optimization of filament geometry and fiber architecture for a given control goal

---

**Require:**  $\mathcal{M}_{\mathbb{E}}$ , ▷ Scheme for expected imp. maximization within Bayesian optimization  
 $\mathcal{C}_{\mathcal{P}}$ , ▷  $\mathcal{C}_{\mathcal{P}}$  = Constraints on  $\mathcal{P}$   
 $\tilde{n}_{\text{prior}}, n_{\text{prior}}, O = \{\epsilon_J, \epsilon_f, \mathbf{Z}_{\min}, \mathbf{Z}_{\max}\}$ , ▷ Auxiliary optimization hyperparameters  
 $\mathcal{G} = \{\mathcal{G}, \mathcal{C}_{\Gamma}, J^{\mathcal{G}}(\mathcal{B}_{\mathbb{A}}), \mathcal{Z}, \mathcal{S}\}$  ▷ Control objective specification

$\mathcal{X}_{\mathcal{P}} \leftarrow$  feasible set of  $\mathcal{P}$ , as defined by  $\mathcal{C}_{\mathcal{P}}$   
 $\mathcal{X} \leftarrow$  Sobol quasi-random sampling plan over  $\mathcal{X}_{\mathcal{P}}$   
 $\mathcal{P}_1^{\text{prior}}, \dots, \mathcal{P}_{\tilde{n}_{\text{prior}}}^{\text{prior}} \leftarrow \tilde{n}_{\text{prior}}$  samples from  $\mathcal{X}$   
 $f_j^{\text{prior}} \leftarrow f(\mathcal{G}, \mathcal{P}_j^{\text{prior}}; O), \forall j \in \{1, \dots, n_{\text{prior}}\}$  ▷ Parallelized computation of priors  
 $\{(\mathcal{P}_j^{\text{prior}}, f_j^{\text{prior}})\} \leftarrow$  Discard  $\{(\mathcal{P}_j^{\text{prior}}, f_j^{\text{prior}})\}$  with  $f_j^{\text{prior}} > \epsilon_f$  or  $J^{\mathcal{G}}(\mathbf{r}(Z; \boldsymbol{\Gamma}^{\mathcal{G}}, \mathcal{P}_j^{\text{prior}})) > \epsilon_J$ ,  
where  $\boldsymbol{\Gamma}^{\mathcal{G}} = \text{Algorithm 1}(\mathcal{G}, \mathcal{P}_j^{\text{prior}}), \forall j \in \{1, \dots, \tilde{n}_{\text{prior}}\}$   
 $H^{\text{prior}} \leftarrow$  First  $n_{\text{prior}}$  samples from  $\{(\mathcal{P}_1^{\text{prior}}, f_1^{\text{prior}}), \dots, (\mathcal{P}_{\tilde{n}_{\text{prior}}}^{\text{prior}}, f_{\tilde{n}_{\text{prior}}}^{\text{prior}})\}$   
 $\mathcal{P}^* \leftarrow \text{Bay arg min}_{\mathcal{P}} (f(\mathcal{G}, \mathcal{P}; O), \text{ with } \mathcal{P} \in \mathcal{X}_{\mathcal{P}},$   
and the priors  $H^{\text{prior}}$ , with scheme  $\mathcal{M}_{\mathbb{E}}$  for expected imp. maximization) ▷  $f = \text{Algorithm 3}$ , Bay min = **Algorithm 4**

---

#### 4.5. Selection of the scheme $\mathcal{M}_{\mathbb{E}}$ for maximization of the expected improvement

Prototypical investigation of the Bayesian optimization performance in solving (26) showed that direct optimization methods—including the simulated annealing and Nelder-Mead simplex algorithms—are not computationally viable for the  $\mathcal{M}_{\mathbb{E}}$  scheme. Specifically, when either simulated annealing or Nelder-Mead is used for constrained maximization of the expected improvement

---

**Algorithm 6** Maximization scheme  $\mathcal{M}_{\mathbb{E}}$  for the expected improvement in Bayesian optimization

---

**Require:** GP ▷ Current Gaussian process

$f_{\min}$  ▷ Minimum value of  $f$  identified so far

$n_{\mathbb{E}}$  ▷ Number of samples in the interior sampling plan over  $\mathcal{X}_{\mathcal{P}}$

$\mathcal{X}_{\text{GP}} \leftarrow |\mathcal{P}|\text{-dimensional Sobol quasi-random sampling plan over } \mathcal{X}_{\mathcal{P}}$  with  $n_{\mathbb{E}}$  samples

$(\partial\mathcal{X}_{\text{GP}})_i \leftarrow (|\mathcal{P}| - 1)\text{-dimensional Sobol quasi-random sampling plan over the } i\text{-th boundary}$   
of  $\mathcal{X}_{\mathcal{P}}$  with  $n_{\mathbb{E}}^{(|\mathcal{P}|-1)/|\mathcal{P}|}$  samples (rounded to the nearest int.),  $\forall i \in \{1, \dots, 2|\mathcal{P}|\}$   
▷ Re-seeded before every sampling plan construction

$\mathcal{X}_{\text{GP}} \leftarrow \mathcal{X}_{\text{GP}} \cup \left( \bigcup_{i=1}^{2|\mathcal{P}|} (\partial\mathcal{X}_{\text{GP}})_i \right)$

$\hat{\mu}(\mathcal{P}), \hat{\sigma}(\mathcal{P}) \leftarrow$  Predicted mean and standard deviation functions of the GP

$\mathbb{E}[\text{Imp}(f(\mathcal{G}, \mathcal{P}))] \leftarrow \mathbb{E}(\mathcal{P}) = (f_{\min} - \hat{\mu}(\mathcal{P}))P(f \leq f_{\min}) + \hat{\sigma}(\mathcal{P})^2 \mathcal{N}(f_{\min} | \hat{\mu}, \hat{\sigma}^2)$   
▷ adapted from [30],  $P(f \leq f_{\min})$  = probability of improvement

$\{\mathbb{E}(\mathcal{P}_1), \dots, \mathbb{E}(\mathcal{P}_{|\mathcal{X}_{\text{GP}}|})\} \leftarrow$  Evaluate  $\mathbb{E}$  for all  $\mathcal{P} \in \mathcal{X}_{\text{GP}}$ , in parallel

$\mathcal{P}^{\text{new}} \leftarrow \arg \max_{\mathcal{P}} \{\mathbb{E}(\mathcal{P}_1), \dots, \mathbb{E}(\mathcal{P}_{|\mathcal{X}_{\text{GP}}|})\}$  ▷ Maximize expected improvement over the sampling plan

---

with  $\mathcal{P} \in \mathcal{X}_{\mathcal{P}}$ , the associated computational overhead becomes too significant compared to the cost of a single evaluation of  $f$ . Thus, choosing these methods would compromise the effectiveness of Bayesian optimization. Even if  $\mathcal{M}_{\mathbb{E}}$  is further augmented to allow for  $n_{\text{core}}$  randomized and parallelized restarts—similar to the augmented approach taken in evaluating  $f$ —the solutions computed by these schemes frequently violate the control quality condition  $J^{\mathcal{G}} \leq \epsilon_J$ .

**Remark.** A potential justification for the poor performance of direct methods is that, since  $\mathcal{E}^{\mathcal{G}}$  is erratically multi-valued, as discussed in Section 5.2, and because it exhibits extreme non-convexity within all of its branches and over a large range of length scales in  $\mathcal{P}$ -space, the fitted Gaussian process approximation of  $f$  also becomes highly sensitive to small changes in  $\mathcal{P}$ . This renders the constrained direct search for the maximizer computationally expensive.

Nevertheless, high-fidelity maximization of the expected improvement is not necessary for satisfactory performance of Bayesian optimization. Further testing revealed that maximizing the expected improvement over a discrete set of samples  $\mathcal{X}_{\text{GP}} \subset \mathcal{X}_{\mathcal{P}}$  provided maximizers that still aided the progression of the Bayesian optimization process, while being less costly than direct methods used with constrained optimization. In particular, we constructed a sampling plan  $\mathcal{X}_{\text{GP}}$  using a  $|\mathcal{P}|$ -dimensional Sobol quasi-random sequence. We further introduced additional Sobol sampling plans on the  $(|\mathcal{P}| - 1)$ -dimensional hyperplane boundaries of  $\mathcal{X}_{\mathcal{P}}$ , so that the maximization occurs over a low-discrepancy set with well-resolved expectation data on the boundaries. To preserve an approximately constant sampling density over both the volume and boundaries of  $\mathcal{X}_{\mathcal{P}}$ , we drew  $n_{\mathbb{E}}$  samples in the interior of  $\mathcal{X}_{\mathcal{P}}$ , and placed  $n_{\mathbb{E}}^{(|\mathcal{P}|-1)/|\mathcal{P}|}$  sampling sites on each hyperplane boundary.

**Remark.** While each single evaluation of  $f$  involves parallelized computations that cannot be nested, a single evaluation of the Gaussian process is serial. We thus generate the sample population over  $\mathcal{X}_{\text{GP}}$  by performing all relevant Gaussian process evaluations in parallel. This permits denser sampling plans for approximate maximization of the expected improvement. Algorithm 6 outlines the algorithmic description of the chosen method for  $\mathcal{M}_{\mathbb{E}}$ .

#### 4.6. Performance evaluation

Preliminary analysis lead to the observation that, due to the erratic functional behavior of  $\mathcal{E}^g$ , large amounts of noise are present in the data set formed by all evaluations of the objective  $f$  during Bayesian optimization. Thus, a plot of the function evaluation history would enable only qualitative conclusions based on the graphical spread of the data along the  $f$  axis. To facilitate quantitative evaluation, we introduce two additional metrics to assess the performance of the Bayesian optimization approach compared to a random search baseline.

Our first performance evaluation metric considers the distribution of the objective function values within several windows of the optimization process, given that the objective evaluations within Bayesian minimization can generally exhibit a high degree of randomness. Specifically, we fit a set of  $K_d$  distributions to a set of  $K_d$  iteration partitions of the Bayesian optimization to observe the distribution-wise progression of the objective function evaluations. We compare the set of distributions against the distribution of a random search baseline, for which we compute a large number  $\tilde{n}_{\text{rand}}$  of evaluation points using a Sobol sequence-based sampling plan over  $\mathcal{X}_{\mathcal{P}}$ . The random samples undergo post-processing akin to the set of priors in Algorithm 5 to preserve a total of  $n_{\text{rand}}$  samples with  $f \leq \epsilon_f$  and  $J^g \leq \epsilon_J$ .

The second metric is inspired by the acceleration factor benchmarking approaches [31]. It is the lowest iteration index at which the minimum objective value found by the algorithm so far is no larger than a given threshold  $f_{\text{th}}$ . In other words, the minimum of  $f$  found so far is first computed as a function of the iteration index  $k$ ,

$$f_{\text{best}}(k) = \min\{f_{[1]}, \dots, f_{[k]}\}, \quad k \in \{1, \dots, K\}, \quad (28)$$

where  $f_{[k]}$  is the value of the objective function at the  $k$ -th iteration. Then, we define the second performance metric as

$$\mathcal{K}_{\min}(f_{\text{th}}) = \arg \min_{k \in \{1, \dots, K\}} (f_{\text{best}}(k), \text{ s.t. } f_{\text{best}}(k) \leq f_{\text{th}}). \quad (29)$$

The metric in (29) is a function of  $f_{\text{th}}$  both for the Bayesian optimization algorithm and for a random search baseline.  $\mathcal{K}_{\min}(f_{\text{th}})$  constitutes a rough estimate of the convergence capabilities of the Bayesian optimization method when applied to (26), with lower values of  $\mathcal{K}_{\min}$  indicating better convergence properties at a given  $f_{\text{th}}$ .

## 5. Results and Discussion

Our proposed optimization methodology is general, and applies to arbitrary fiber-based slender actuators and control objective specifications. Since benchmarking our approach for all possible actuation paradigms is a complex task, here, we focus on evaluating the methodology for a single target endpoint position, as in (18). Notably, our analysis generalizes to any other actuation requirements, beyond any simplifying assumptions that we make in this evaluation.

### 5.1. Optimization of two-ring actuator geometry and fiber architecture

For better interpretability of the results, we restrict the following analysis to a two-ring,  $M = 2$ , actuator with fixed mechanical properties  $\mathbf{E} = (1, 1)$  and  $\boldsymbol{\nu} = (1/2, 1/2)$ , and a constant length  $L = 10$ . The choice of a fixed ring count  $M$  is necessary since the dimensionality of  $\mathcal{P}$  depends on  $M$  and our implementation assumes a constant dimensionality of  $\mathcal{P}$ . The specific value of the filament length  $L$  is insignificant, since the filament geometry can be expressed in terms of the dimensionless groups involving  $L$ ,  $R_1^{(1)}$  and  $t^{(i)}$ . As a result, the design space consists of all points

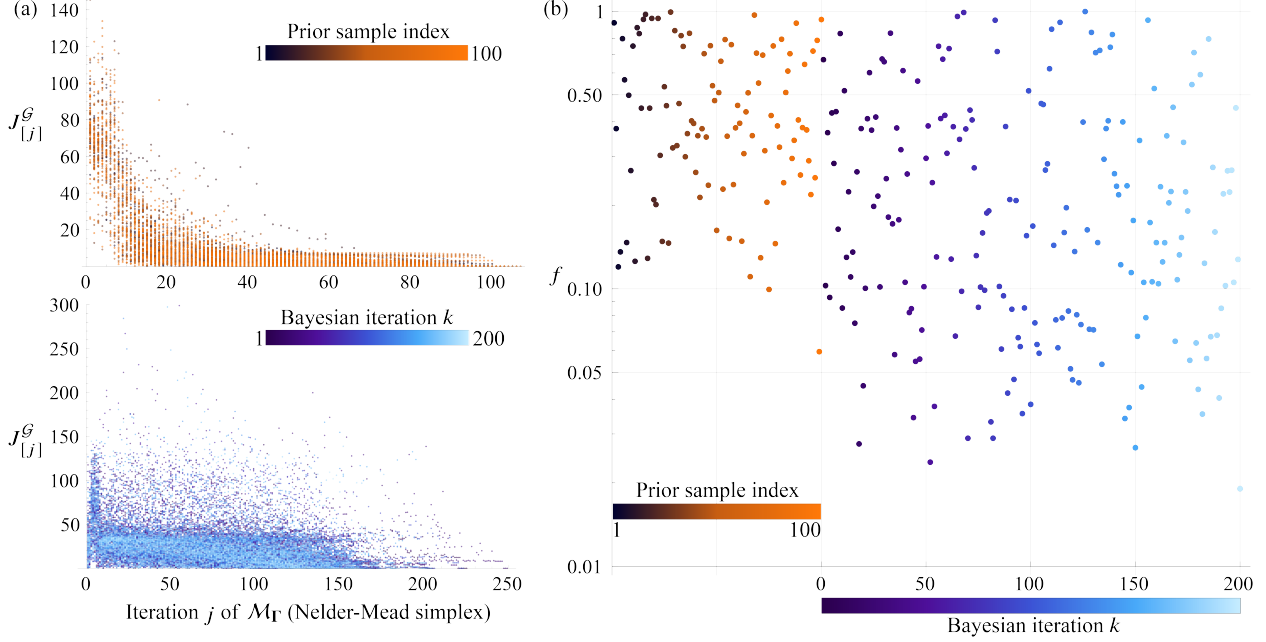


Figure 3: Bayesian design optimization for the prescribed control problem and the chosen feasible set of potential actuator designs. (a) Convergence plots of the control objective cost function  $J^G$  for prior sample generation (top) and the Bayesian optimization (bottom). Every evaluation of the objective function  $f$  involves solving an optimization problem. The top plot visualizes  $n_{\text{prior}} = 100$  convergence data sets for the prior sample generation; the bottom plot shows 200 convergence data sets for the  $K = 200$  iterations of the Bayesian optimization. (b) Evaluation history for the objective function  $f$  for both the prior samples (left), and the Bayesian optimization (right). The colors of the individual data points correspond to the data sets in the  $J^G$  convergence plots in (a).

$\mathcal{P} = \mathcal{D} \cup \mathcal{F} = \{R_1^{(1)}, \mathbf{t}, \boldsymbol{\alpha}_2, \boldsymbol{\sigma}, \mathbf{N}, \boldsymbol{\theta}_2\}$ , and we seek to optimize the geometry and fiber architecture of the two-ring actuator over all feasible  $\mathcal{P}$ . We define the feasible set through the element-wise inequality  $\mathcal{P}_{\min} \leq \mathcal{P} \leq \mathcal{P}_{\max}$ , where  $\mathcal{P}_{\min} = \{0.2, (0.02, 0.02), (0, 0), \frac{1}{12}(\pi, \pi), (1, 1), (0, 0)\}$  and  $\mathcal{P}_{\max} = \{0.5, (0.2, 0.2), \frac{1}{4}(\pi, \pi), \frac{1}{4}(\pi, \pi), (4, 4), (0, 2\pi - \pi/64)\}$ . The  $Z = 0$  endpoint of the actuator is clamped at the origin, with boundary conditions  $\mathbf{r}^0 = (0, 0, 0)$ , and  $\mathbf{D}^0 = \{\mathbf{e}_X, \mathbf{e}_Y, \mathbf{e}_Z\}$ . To ensure that the fixed orientation of the cross section at the  $Z = 0$  boundary is meaningful, the design variable  $\theta_0^{(1)}$  is set to vanish, since permitting arbitrary values of both  $\theta_0^{(1)}$  and  $\theta_0^{(2)}$  is equivalent to removing the  $\mathbf{D}^0$  boundary condition. The actuator seeks to fulfill a control objective specification  $\mathcal{G}$  as defined in (18) by reaching a target endpoint position  $\mathbf{r}_{\text{end}}^G = \frac{1}{3}(L, L, L)$ . The constraint set  $\mathcal{C}_{\Gamma}$  is empty, i.e., no constraints are imposed on  $\Gamma$  beyond the ones implicitly affecting the ultimate values of  $\Gamma^G$  through the  $J^G \leq \epsilon_J$  and  $f \leq \epsilon_f$  conditions. We set the threshold defining satisfactory control to  $\epsilon_J = 10^{-3}$ , and the maximum permissible objective value to  $\epsilon_f = 1$ . We evaluate a total of  $n_{\text{prior}} = 100$  priors and the Bayesian optimization is performed for  $K = 200$  iterations. The remaining hyperparameters are chosen as  $n_{\text{init}} = 2$ ,  $n_{\mathbb{E}} = 400$ ,  $N_{\text{res}} = 20$ , and  $\mathbf{Z}_{\min/\max} = \mp[3, \dots, 3] \in \mathbb{R}^{\sum_i N^{(i)}}$ . Due to the computational cost of the entire Bayesian optimization process, we hand-tune all hyperparameters, including  $\mathcal{M}_{\Gamma}$ , for smaller values of  $K$  until robust optimization performance is achieved. We select the Nelder-Mead simplex method as the optimization scheme  $\mathcal{M}_{\Gamma}$  in Algorithm 1.

Fig. 3 summarizes the results of Bayesian optimization of the actuator's geometry and fiber architecture under the prescribed control objective specification. Fig. 3a shows the convergence plots of the Nelder-Mead simplex method in Algorithm 1 for all prior samples and all evaluations of  $f$  throughout Bayesian optimization, which corresponds to  $n_{\text{prior}} = 100$  convergence curves

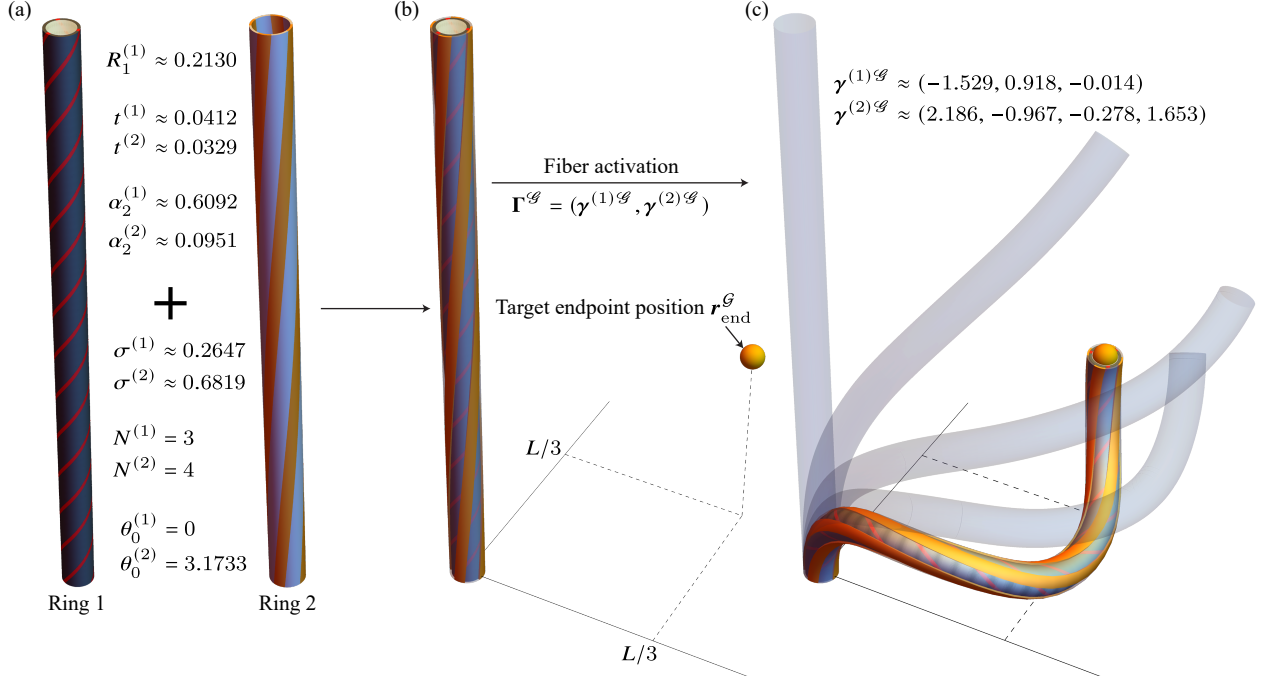


Figure 4: The most optimal actuator design identified during the Bayesian optimization procedure, under the imposed control objective specification. (a) Visualization of the rings comprising the two-ring actuator, together with the parameters defining the geometries and fiber architectures of the two rings. (b) The complete two-ring actuator with a schematic of the control objective specification. (c) The deformed configuration of the most energetically optimal actuator that successfully matches the prescribed control objective. The translucent filamentary outlines depict a control path (linearly interpolated in  $\Gamma$ -space) that could be taken by the actuator to reach the target position.

for the priors, and  $K = 200$  convergence curves for the evaluations during Bayesian optimization. Acceptable convergence in the  $\Gamma$ -space is observed for all prior samples after roughly 100 iterations, and for almost all evaluations of  $f$  after approximately 150 iterations of  $\mathcal{M}_\Gamma$ . We emphasize that the plots only depict the convergence curves for which the condition  $J^G \leq \epsilon_J$  is met at the last iteration of  $\mathcal{M}_\Gamma$ , since the sample is discarded otherwise both in the prior set and during Bayesian optimization. Most of the  $\mathcal{M}_\Gamma$  executions exhibit fast convergence of  $J^G$  close to the last iteration and slower convergence in earlier iterations, as the hyperparameters of the Nelder-Mead method are set to promote exploration of the functional landscape to more robustly identify the global minima.

Fig. 3b visualizes the progression of the objective values  $f$  evaluated throughout the Bayesian optimization process as a function of the Bayesian iteration  $k$ , together with the  $f$  values computed for the set of priors. As expected, the evaluations during Bayesian optimization are scattered along the  $f$ -axis and no clear convergence pattern is present throughout the entire sequence of  $K$  iterations. Nonetheless, it is evident that the Bayesian optimization identifies smaller values of  $f$  more effectively than the randomized sampling in the set of priors. Fig. 4 demonstrates the actuator design associated with the smallest identified value of the objective function  $f$ , along with the actuator's deformed configuration that achieves the specified control objective. The actuator design  $\mathcal{P}$  that achieves this minimal energetic cost of activation  $f$  is defined by the parameters  $R_1^{(1)} \approx 0.2130$ ,  $t \approx (0.0412, 0.0329)$ ,  $\alpha_2 \approx (0.6092, 0.0951)$ ,  $\sigma \approx (0.2647, 0.6819)$ ,  $N \approx (3, 4)$ , and  $\theta_0 \approx (0, 3.1733)$ . Since Fig. 3b does not demonstrate a clear convergence trend, the actuator in Fig. 4 merely corresponds to the smallest identified value of  $f$  throughout  $K$  iterations of the

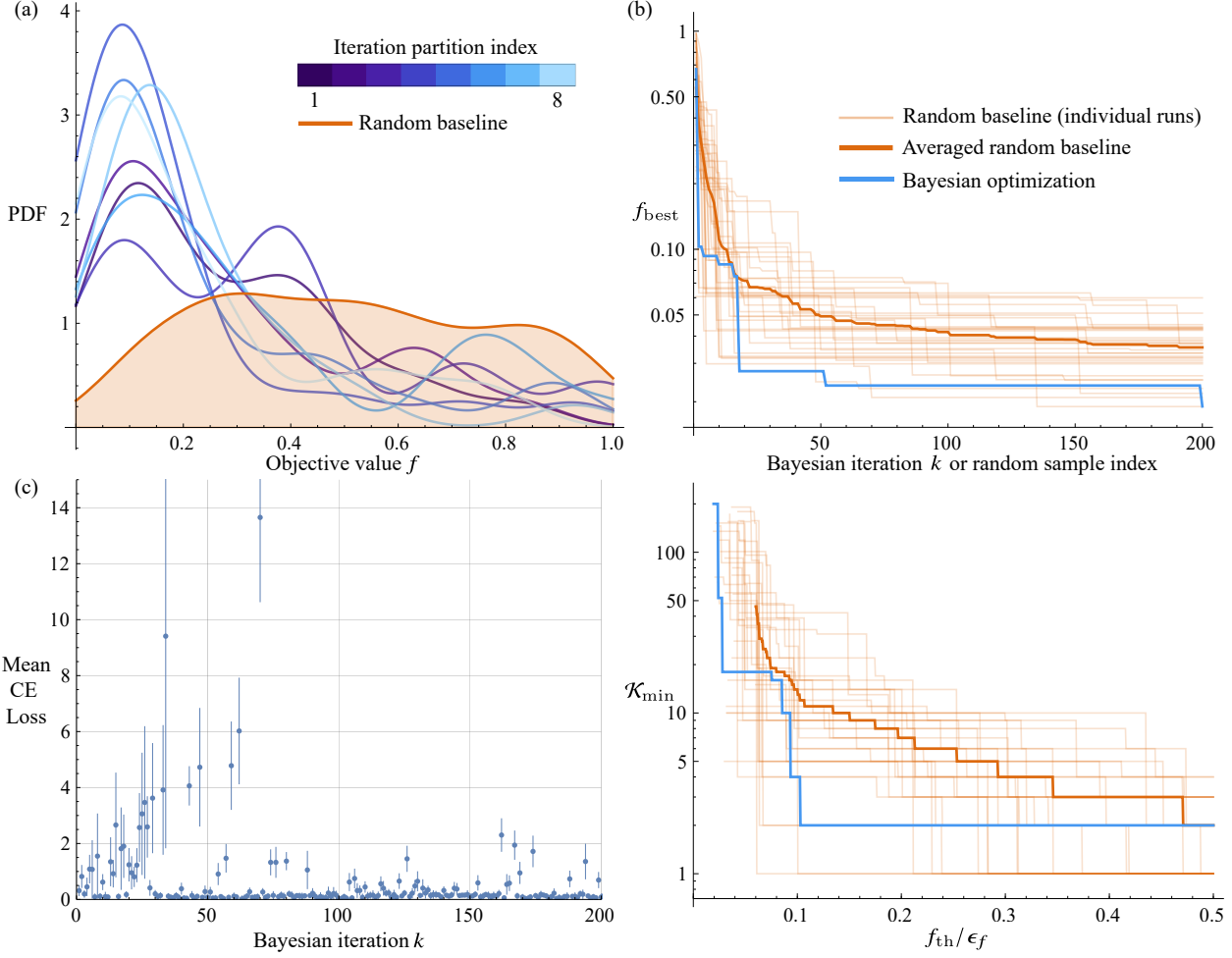


Figure 5: Performance of the proposed Bayesian optimization method. (a) Truncated smooth kernel distributions of the objective function evaluations for a random baseline with  $n_{\text{rand}} = 1000$  samples, and for  $K_d = 8$  iteration partitions. The Bayesian optimization identifies design points with smaller objective function values  $f$  more frequently than the random baseline method. (b) Top: minimum objective function value  $f_{\text{best}}$  as a function of the Bayesian iteration  $k$  and the index of the random sample in each of the 32 randomized runs with  $n_{\text{rand}} = 200$  samples. Bottom:  $K_{\min}$  metric as a function of the normalized energetic threshold  $f_{\text{th}}/\epsilon_f$  for both the random baseline and the Bayesian optimization method. The curves for the Bayesian optimization method never exceed the averaged random baseline curves, which indicates that the utilized method finds design points with smaller  $f$  in a fewer number of iterations. (c) Mean cross-entropy loss as a function of the Bayesian iteration index  $k$ . The Gaussian process fits the evaluation history better and with higher confidence at later iterations. The plot is cropped along the vertical axis to more clearly visualize smaller values of the mean cross-entropy loss.

Bayesian optimization process, and it is neither a global nor a local minimum of  $f$ .

To evaluate whether the Bayesian optimization is more effective at minimizing  $f$  than randomized sampling, we visualize the distribution of the optimization data set  $f$  over  $K_d = 8$  contiguous partitions of equal length, and compare the result to a quasi-random baseline generated for  $n_{\text{rand}} = 1000$  post-processed evaluations. For each partition, Fig. 5a shows the probability density functions of smooth kernel distributions truncated to  $f \in [0, \epsilon_f]$  together with the truncated smooth kernel distribution of the random baseline. Based on the computed distributions, the Bayesian optimization identifies designs with smaller objective function values much more frequently than the random baseline approach. Interestingly, the distributions of  $f$  in the Bayesian

optimization have multi-modal characteristics, which might be related to the multiple branches of the energetic activation cost function  $\mathcal{E}^{\mathcal{G}}$ .

To further support the advantages of the proposed optimization method, we compute the performance metric  $\mathcal{K}_{\min}(f_{\text{th}})$  for both the Bayesian optimization results and the random baseline. In particular, Fig. 5b (top) shows the minimum function value  $f_{\text{best}}$  up until iteration  $k$  for the Bayesian optimization, and for a set of 32 randomized sampling runs with  $n_{\text{rand}} = 200$  samples each. Based on the computed  $f_{\text{best}}(k)$  curves, we generate the curves of the  $\mathcal{K}_{\min}(f_{\text{th}})$  metric, and plot them in Fig. 5b (bottom) with  $f_{\text{th}} \in [0.005\epsilon_f, 0.5\epsilon_f]$ , for both the Bayesian optimization and randomized cases. Since  $\mathcal{K}_{\min}(f_{\text{th}}) \in \mathbb{Z}_+$ , we compute the averaged  $\mathcal{K}_{\min}$  curves with a ceiling operation to consider the conservative case of the  $\mathcal{K}_{\min}(f_{\text{th}})$  metric. The random baseline curves  $f_{\text{best}}(k)$  and  $\mathcal{K}_{\min}(f_{\text{th}})$  averaged over the 32 randomized runs both lie consistently above the respective  $f_{\text{best}}(k)$  and  $\mathcal{K}_{\min}(f_{\text{th}})$  curves obtained for the Bayesian optimization process, which suggests that Bayesian optimization identifies optimal actuator designs faster than a randomized sampling, in addition to doing so more frequently.

Last, we evaluate the quality of the Gaussian process fit throughout the Bayesian optimization in the investigated scenario by considering the mean cross-entropy loss of the Gaussian process training as a function of the optimization iteration  $k \in \{1, \dots, K\}$ . Fig. 5c shows the plot of the mean cross-entropy loss of the Gaussian process, where each error bar corresponds to the standard deviation of the cross-entropy loss at iteration  $k$ . If we neglect the outliers, based on the mean cross-entropy loss data, the Gaussian process surrogate model fits the evaluation history better at later iterations  $k$  in the Bayesian optimization, and is more confident in the quality of the fit at later iterations as well. This behavior is consistent with the expectation that the chaotic functional nature of  $f$  is approximated more accurately as more data are added to the evaluation history.

## 5.2. Non-invertibility of the mapping $\mathbb{A}$

The existence of the inverse  $\mathbb{A}_{\Gamma}^{-1}$  of the mapping  $\mathbb{A}$  with respect to  $\Gamma$  is governed by a highly complex function of both  $\mathcal{G}$  and  $\mathcal{C}_{\Gamma}$ . In almost all cases, the mapping  $\mathbb{A}$  is not invertible with respect to  $\Gamma$ . There generally exists an infinite number of activation parameter sets  $\Gamma$  that produce the same configuration  $\mathcal{B}_{\mathbb{A}}$ , so there also exists an infinite number of parameter sets  $\Gamma$  that globally minimize the control cost function  $J^{\mathcal{G}}(\mathcal{B}_{\mathbb{A}})$ . As such, a hypothetical, infinitely robust global optimization method that always converges to a global minimum of  $J^{\mathcal{G}}$  can still yield different optimal activation sets  $\Gamma^{\mathcal{G}}$  under different initializations or due to algorithmic stochasticity. Regardless of the robustness of the schemes  $\mathcal{M}_{\Gamma}$  and  $\mathcal{M}_{\mathbb{E}}$ , this behavior has a negative effect on the optimization of  $f$ , because different  $\Gamma^{\mathcal{G}}$  generally result in different energetic costs  $\mathcal{E}^{\mathcal{G}}$  for the same filament definition  $\mathcal{P}$ . In fact, the same specification  $\mathcal{G}$  and filament definition  $\mathcal{P}$  can yield optimal  $\mathcal{E}^{\mathcal{G}}$  of vastly differing magnitudes, depending on the optimum computed by Algorithm 1. Consequently,  $\mathcal{E}^{\mathcal{G}}$  is generally highly multi-valued over any feasible set of  $\mathcal{P}$ , with the range of  $\mathcal{E}^{\mathcal{G}}$  spanning all of  $\mathbb{R}_+$ .

To illustrate the multi-valued nature of the optimal energetic cost  $\mathcal{E}^{\mathcal{G}}$ , we consider a simple single-ring filament geometry with a variable inner radius  $R_1^{(1)}$ , for six uniformly spaced helical fiber angles  $\alpha_2^{(1)} \in [\pi/12, \pi/4]$ , and all other parameters in  $\mathcal{P}$  held fixed. The values of  $\mathcal{E}^{\mathcal{G}}$  are then computed for the  $\mathcal{G}$  specification in Section 5.1, for a large number of random  $R_1^{(1)}/L \in [0.02, 0.05]$ , with multiple randomized initializations in  $\mathcal{M}_{\Gamma}$ . Fig. 6 shows the resulting plots of  $\mathcal{E}^{\mathcal{G}}$  as a function of  $R_1^{(1)}$  for each of the six helical fiber angles, with  $\mathcal{E}^{\mathcal{G}}$  plotted on a logarithmic scale. The plots highlight numerous branches of the multi-valued  $\mathcal{E}^{\mathcal{G}}$  for all evaluated helical angles and, to add to the complexity of the functional nature of  $\mathcal{E}^{\mathcal{G}}$ , solution branches can intersect one another arbitrarily without any clear patterns. It is worth noting that, in the case of a 1-dimensional design space,

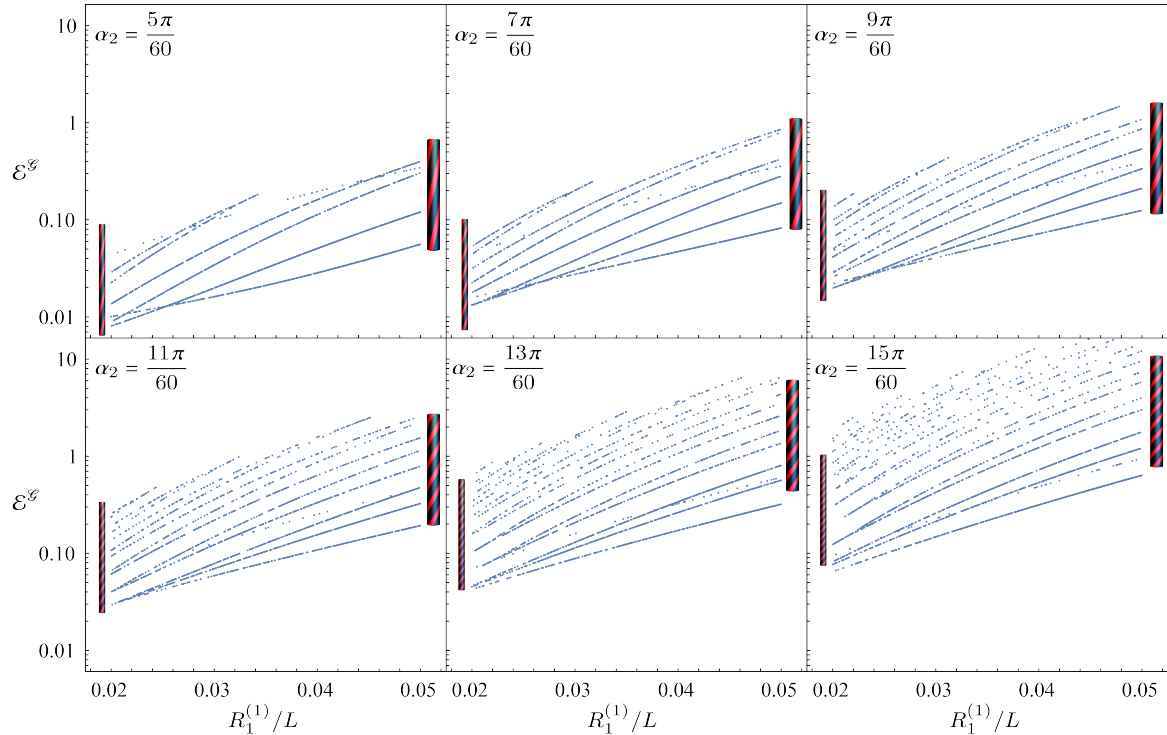


Figure 6: Multi-valued energetic cost  $\mathcal{E}^{\mathcal{G}}$  as a function of the normalized inner radius  $R_1^{(1)}$  of a single-ring filament, for six different helical angle values. Multiple solution branches exist for a single design point, which introduces computational challenges in the Bayesian optimization process. We define the actuator with the fixed properties  $t/L = 0.01$ ,  $\sigma = \pi/4$ ,  $N = 3$ ,  $\theta_0 = 0$ ,  $E = 1$ , and  $\nu = 0.5$  in its single ring. The energetic cost was computed under the control objective specification used in Section 5.1.

each branch is represented by a curve. In the general case, however, the range of the multi-valued  $\mathcal{E}^{\mathcal{G}}$  can be represented by an infinite number of  $|\mathcal{P}|$ -dimensional manifolds over  $\mathcal{X}_{\mathcal{P}}$ .

The multi-valuedness of  $\mathcal{E}^{\mathcal{G}}$  introduces undesirable noise into the Gaussian process, since subsequent evaluations might switch between branches of  $\mathcal{E}^{\mathcal{G}}$  in an uncontrollable manner. As a result, the Gaussian process might make predictions based on a chaotic mixture of the various branches of  $\mathcal{E}^{\mathcal{G}}$ , which can significantly reduce its performance in Bayesian optimization, as manifested in the scattered distribution of  $f$  values throughout the optimization process in Fig. 3b. At the same time, the multi-valued nature of  $\mathcal{E}^{\mathcal{G}}$  also supports the choice of Bayesian minimization as the primary method in our approach, because it is known to be a suitable method for optimizing non-deterministic functions. The large range of values that  $\mathcal{E}^{\mathcal{G}}$  can take at a single design  $\mathcal{P}$  and specification  $\mathcal{G}$  is also the reason for filtering out any outliers  $f > \epsilon_f$  in both the construction of the prior evaluation history  $H^{\text{Prior}}$ , and during Bayesian optimization. It is currently unclear how we could robustly mitigate this overall challenge, and any potential computational remedies will need further investigation.

## 6. Conclusions

The development of a robust design approach for soft actuators remains a formidable engineering challenge. So far, most studies have considered quantitative methodologies for identifying optimal

soft-robotic designs, but these approaches are computationally expensive or consider a limited family of design objectives motivated by the actuation goals of specific engineering prototypes.

As an alternative, we formulated a automated method for the design optimization of fiber-based soft actuators that can be easily generalized. In our method, we minimize the energetic actuation cost under arbitrary control objectives based on a desired robotic functionality. To address the excessive computational cost associated with the objective function and its multi-valued nature, we applied Bayesian minimization as the method of choice to construct the optimization procedure. Notably, even though the computational cost for the evaluation of the objective function warranted using a surrogate optimization approach, our optimization methodology is computationally inexpensive compared to other common design optimization approaches. We evaluated systematically our proposed optimization method for the specific control objective of reaching a target endpoint position, and determined the most favorable actuator design for that objective. Our methodology performed better than a random baseline method for this investigated scenario. More importantly, our approach is formulated in a way that can be easily extended to search for soft actuator designs that maximize robotic adaptability and actuation versatility under a large set of control objectives, while maintaining computational feasibility.

Our study of Bayesian optimization, as applied to soft actuator design, exhibits some noteworthy limitations. First, our activation optimization method for actuator control relies on the assumption of quasi-static motion. The quasi-static assumption renders our approach applicable only to actuator deformations where inertial forces can be neglected. To address this limitation, we could incorporate filament dynamics into the model mapping  $\mathbb{A}$ , and develop a model-based framework for feedback control of active filaments. Second, our approach is primarily heuristic in identifying the most desirable branch of the multi-valued energy function. To make Bayesian minimization of the energy more robust, we could develop a less generic optimization scheme  $\mathcal{M}_{\Gamma}$  directly informed by the physics embedded in the active filament model. Third, the rate of convergence of our Bayesian optimization method is sensitive to the choice of hyperparameters. To address this effect, we could conduct a sensitivity study to isolate the hyperparameters with the highest impact on convergence, or reformulate the post-processing steps of our methodology to reduce the number of hyperparameters, which is a challenging task.

To further reinforce the validity of our results, several independent data sets could be obtained for the Bayesian optimization process, so that curves averaged over multiple optimization runs can be compared against the random baseline method. Moreover, to assess the performance of our optimization methodology in identifying designs that ensure a high degree of robotic adaptability, we could adopt a more involved control objective specification  $\mathcal{G}$ . Specifically, we could incorporate a weighted multi-objective formulation with several specifications  $\mathcal{G}_i$ , so that the energy-optimized actuator performs well under multiple actuation paradigms. Finally, implementing the additional capability of optimizing with respect to the number of actuator rings  $M$  would enlarge the design space to encompass significantly more complex structures.

The universal nature of the active filament model not only enables more exhaustive optimization of fiber-based soft actuators, but also provides insight into the mechanical principles that govern optimal soft actuation. In combination with the state-of-the-art approaches in soft robotics, our generalized framework can serve as a powerful tool for the prototyping, design, fabrication, and operation of soft devices.

## Acknowledgments

The work of AG was supported by the Engineering and Physical Sciences Research Council grant EP/R020205/1 to AG.

## Declaration of competing interest

The authors declare that they have no known competing financial interests or personal relationships that could have appeared to influence the work reported in this paper.

## References

- [1] D. Rus, M. T. Tolley, Design, fabrication and control of soft robots, *Nature* 521 (7553) (2015) 467–475. doi:[10.1038/nature14543](https://doi.org/10.1038/nature14543).
- [2] C. Della Santina, R. K. Katzschmann, A. Biechi, D. Rus, Dynamic control of soft robots interacting with the environment, in: 2018 IEEE International Conference on Soft Robotics (RoboSoft), 2018, pp. 46–53. doi:[10.1109/ROBOSOFT.2018.8404895](https://doi.org/10.1109/ROBOSOFT.2018.8404895).
- [3] D. Trivedi, D. Dienno, C. D. Rahn, Optimal, Model-Based Design of Soft Robotic Manipulators, *Journal of Mechanical Design* 130 (9) (Aug. 2008). doi:[10.1115/1.2943300](https://doi.org/10.1115/1.2943300).
- [4] A. W. Feinberg, Biological Soft Robotics, *Annual Review of Biomedical Engineering* 17 (1) (2015) 243–265. doi:[10.1146/annurev-bioeng-071114-040632](https://doi.org/10.1146/annurev-bioeng-071114-040632).
- [5] M. W. Hannan, I. D. Walker, Kinematics and the Implementation of an Elephant's Trunk Manipulator and Other Continuum Style Robots, *Journal of Robotic Systems* 20 (2) (2003) 45–63. doi:[10.1002/rob.10070](https://doi.org/10.1002/rob.10070).
- [6] J. Yang, E. P. Pitarch, J. Potratz, S. Beck, K. Abdel-Malek, Synthesis and analysis of a flexible elephant trunk robot, *Advanced Robotics* 20 (6) (2006) 631–659. doi:[10.1163/156855306777361631](https://doi.org/10.1163/156855306777361631).
- [7] M. K. Mishra, A. K. Samantaray, G. Chakraborty, A. Jain, P. M. Pathak, R. Merzouki, Dynamic Modelling of an Elephant Trunk Like Flexible Bionic Manipulator, in: ASME 2019 International Mechanical Engineering Congress and Exposition, American Society of Mechanical Engineers Digital Collection, 2020. doi:[10.1115/IMECE2019-11113](https://doi.org/10.1115/IMECE2019-11113).
- [8] Q. Guan, J. Sun, Y. Liu, N. M. Wereley, J. Leng, Novel Bending and Helical Extensible/Contractile Pneumatic Artificial Muscles Inspired by Elephant Trunk, *Soft Robotics* 7 (5) (2020) 597–614. doi:[10.1089/soro.2019.0079](https://doi.org/10.1089/soro.2019.0079).
- [9] M. Calisti, M. Giorelli, G. Levy, B. Mazzolai, B. Hochner, C. Laschi, P. Dario, An octopus-inspired solution to movement and manipulation for soft robots, *Bioinspiration & Biomimetics* 6 (3) (2011) 036002. doi:[10.1088/1748-3182/6/3/036002](https://doi.org/10.1088/1748-3182/6/3/036002).
- [10] K. Nakajima, H. Hauser, R. Kang, E. Guglielmino, D. Caldwell, R. Pfeifer, A soft body as a reservoir: Case studies in a dynamic model of octopus-inspired soft robotic arm, *Frontiers in Computational Neuroscience* 7 (2013).
- [11] F. Renda, M. Giorelli, M. Calisti, M. Cianchetti, C. Laschi, Dynamic Model of a Multibending Soft Robot Arm Driven by Cables, *IEEE Transactions on Robotics* 30 (5) (2014) 1109–1122. doi:[10.1109/TRO.2014.2325992](https://doi.org/10.1109/TRO.2014.2325992).
- [12] J. Jiao, S. Liu, H. Deng, Y. Lai, F. Li, T. Mei, H. Huang, Design and Fabrication of Long Soft-Robotic Elastomeric Actuator Inspired by Octopus Arm, in: 2019 IEEE International Conference on Robotics and Biomimetics (ROBIO), 2019, pp. 2826–2832. doi:[10.1109/ROBIO49542.2019.8961561](https://doi.org/10.1109/ROBIO49542.2019.8961561).

- [13] Z. Xie, A. G. Domel, N. An, C. Green, Z. Gong, T. Wang, E. M. Knubben, J. C. Weaver, K. Bertoldi, L. Wen, Octopus Arm-Inspired Tapered Soft Actuators with Suckers for Improved Grasping, *Soft Robotics* 7 (5) (2020) 639–648. doi:10.1089/soro.2019.0082.
- [14] Q. Wu, X. Yang, Y. Wu, Z. Zhou, J. Wang, B. Zhang, Y. Luo, S. A. Chepinskii, A. A. Zhilenkov, A novel underwater bipedal walking soft robot bio-inspired by the coconut octopus, *Bioinspiration & Biomimetics* 16 (4) (2021) 046007. doi:10.1088/1748-3190/abf6b9.
- [15] F. Chen, M. Y. Wang, Design Optimization of Soft Robots: A Review of the State of the Art, *IEEE Robotics Automation Magazine* 27 (4) (2020) 27–43. doi:10.1109/MRA.2020.3024280.
- [16] G. Dämmer, S. Gablenz, A. Hildebrandt, Z. Major, Design and shape optimization of PolyJet bellows actuators, in: 2018 IEEE International Conference on Soft Robotics (RoboSoft), 2018, pp. 282–287. doi:10.1109/ROBOSOFT.2018.8404933.
- [17] H. Zhang, A. S. Kumar, F. Chen, J. Y. H. Fuh, M. Y. Wang, Topology Optimized Multimaterial Soft Fingers for Applications on Grippers, Rehabilitation, and Artificial Hands, *IEEE/ASME Transactions on Mechatronics* 24 (1) (2019) 120–131. doi:10.1109/TMECH.2018.2874067.
- [18] G. Z. Lum, Z. Ye, X. Dong, H. Marvi, O. Erin, W. Hu, M. Sitti, Shape-programmable magnetic soft matter, *Proceedings of the National Academy of Sciences* 113 (41) (2016) E6007–E6015. doi:10.1073/pnas.1608193113.
- [19] F. Chen, K. Liu, Y. Wang, J. Zou, G. Gu, X. Zhu, Automatic Design of Soft Dielectric Elastomer Actuators With Optimal Spatial Electric Fields, *IEEE Transactions on Robotics* 35 (5) (2019) 1150–1165. doi:10.1109/TR0.2019.2920108.
- [20] B. Kaczmarski, D. E. Moulton, E. Kuhl, A. Goriely, Active filaments I: Curvature and torsion generation, *Journal of the Mechanics and Physics of Solids* 164 (2022) 104918. doi:10.1016/j.jmps.2022.104918.
- [21] B. Kaczmarski, A. Goriely, E. Kuhl, D. E. Moulton, Active Filaments II: Physics-informed quasi-static control of biomimetic soft actuators (2022).
- [22] D. E. Moulton, T. Lessinnes, A. Goriely, Morphoelastic rods III: Differential growth and curvature generation in elastic filaments, *Journal of the Mechanics and Physics of Solids* 142 (2020) 104022. doi:10.1016/j.jmps.2020.104022.
- [23] A. Goriely, *The Mathematics and Mechanics of Biological Growth*, Springer Verlag, New York, 2017.
- [24] G. Kirchhoff, Ueber das Gleichgewicht und die Bewegung eines unendlich dünnen elastischen Stabes. 1859 (56) (1859) 285–313. doi:10.1515/crll.1859.56.285.
- [25] D. E. Moulton, T. Lessinnes, A. Goriely, Morphoelastic rods. Part I: A single growing elastic rod, *Journal of the Mechanics and Physics of Solids* 61 (2) (2013) 398–427. doi:10.1016/j.jmps.2012.09.017.
- [26] B. Matérn, *Spatial Variation*, 2nd Edition, no. v. 36 in *Lecture Notes in Statistics*, Springer-Verlag, Berlin ; New York, 1986.
- [27] M. G. Genton, Classes of kernels for machine learning: A statistics perspective, *The Journal of Machine Learning Research* 2 (2002) 299–312.

- [28] C. E. Rasmussen, C. K. I. Williams, Gaussian Processes for Machine Learning, Adaptive Computation and Machine Learning Series, MIT Press, Cambridge, MA, USA, 2005.
- [29] I. M. Sobol', On the distribution of points in a cube and the approximate evaluation of integrals, USSR Computational Mathematics and Mathematical Physics 7 (4) (1967) 86–112. doi: [10.1016/0041-5553\(67\)90144-9](https://doi.org/10.1016/0041-5553(67)90144-9).
- [30] M. J. Kochenderfer, T. A. Wheeler, Algorithms for Optimization, MIT Press, Cambridge, MA, USA, 2019.
- [31] Q. Liang, A. E. Gongora, Z. Ren, A. Tiihonen, Z. Liu, S. Sun, J. R. Deneault, D. Bash, F. Mekki-Berrada, S. A. Khan, K. Hippalgaonkar, B. Maruyama, K. A. Brown, J. Fisher III, T. Buonassisi, Benchmarking the performance of Bayesian optimization across multiple experimental materials science domains, npj Computational Materials 7 (1) (2021) 1–10. doi: [10.1038/s41524-021-00656-9](https://doi.org/10.1038/s41524-021-00656-9).